HHS Public Access

Author manuscript

Neuroimage. Author manuscript; available in PMC 2019 February 15.

Published in final edited form as:

Neuroimage. 2018 February 15; 167: 438–452. doi:10.1016/j.neuroimage.2017.10.063.

Mapping of Thalamic Magnetic Susceptibility in Multiple Sclerosis Indicates Decreasing Iron with Disease Duration: A Proposed Mechanistic Relationship between Inflammation and Oligodendrocyte Vitality

Ferdinand Schweser[1,2,*], **Ana Luiza Raffaini Duarte Martins**[1], **Jesper Hagemeier**[1], **Fuchun Lin**[1], **Jannis Hanspach**[1,3], **Bianca Weinstock-Guttman**[4], **Simon Hametner**[5], **Niels P. Bergsland**[1], **Michael G. Dwyer**[1], and **Robert Zivadinov**[1,2]

[1]Buffalo Neuroimaging Analysis Center, Department of Neurology, Jacobs School of Medicine and Biomedical Sciences, University at Buffalo, The State University of New York, Buffalo, NY

[2]Translational Imaging Center, Clinical and Translational Science Institute, University at Buffalo, The State University of New York, Buffalo, NY, USA

[3]Institute of Radiology, University Hospital Erlangen, Erlangen, Germany

[4]Jacobs Multiple Sclerosis Center, Department of Neurology, Jacobs School of Medicine and Biomedical Sciences, University at Buffalo, The State University of New York, Buffalo, NY, USA

[5]Department of Neuroimmunology, Center for Brain Research, Medical University of Vienna, Vienna, Austria

Abstract

Recent advances in susceptibility MRI have dramatically improved the visualization of deep gray matter brain regions and the quantification of their magnetic properties in vivo, providing a novel tool to study the poorly understood iron homeostasis in the human brain. In this study, we used an advanced combination of the recent quantitative susceptibility mapping technique with dedicated analysis methods to study intra-thalamic tissue alterations in patients with clinically isolated syndrome (CIS) and multiple sclerosis (MS). Thalamic pathology is one of the earliest hallmarks of MS and has been shown to correlate with cognitive dysfunction and fatigue, but the mechanisms underlying the thalamic pathology are poorly understood.

We enrolled a total of 120 patients, 40 with CIS, 40 with Relapsing Remitting MS (RRMS), and 40 with Secondary Progressive MS (SPMS). For each of the three patient groups, we recruited 40 controls, group matched for age- and sex (120 total). We acquired quantitative susceptibility maps using a single-echo gradient echo MRI pulse sequence at 3 Tesla. Group differences were studied by voxel-based analysis as well as with a custom thalamus atlas. We used threshold-free cluster

Corresponding Author: Ferdinand Schweser, PhD, Buffalo Neuroimaging Analysis Center, Department of Neurology, University at Buffalo, 875 Ellicott St., Buffalo, NY 14203, USA, Tel. 716 888 4718, Fax. 716 859 7874, schweser@buffalo.edu.

enhancement (TFCE) and multiple regression analyses, respectively. We found significantly reduced magnetic susceptibility compared to controls in focal thalamic subregions of patients with RRMS (whole thalamus excluding the pulvinar nucleus) and SPMS (primarily pulvinar nucleus), but not in patients with CIS. Susceptibility reduction was significantly associated with disease duration in the pulvinar, the left lateral nuclear region, and the global thalamus. Susceptibility reduction indicates a decrease in tissue iron concentration suggesting an involvement of chronic microglia activation in the depletion of iron from oligodendrocytes in this central and integrative brain region. Not necessarily specific to MS, inflammation-mediated iron release may lead to a vicious circle that reduces the protection of axons and neuronal repair.

Graphical abstract

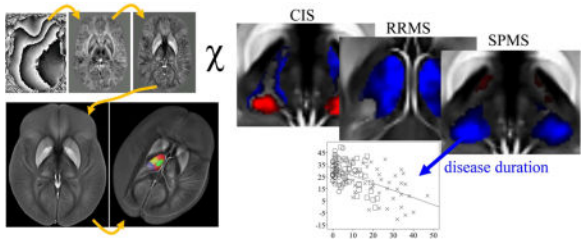

Keywords

quantitative susceptibility mapping; QSM; iron; multiple sclerosis; thalamus

1. Introduction

Atrophy of the thalamus is one of the earliest hallmarks of brain pathology in Multiple Sclerosis (MS) (Audoin et al., 2009; Bergsland et al., 2012; Calabrese et al., 2011; Henry et al., 2009; Henry et al., 2008; Ramasamy et al., 2009; Zivadinov et al., 2013), which correlates with physical disability (Rocca et al., 2010) and fatigue (Calabrese et al., 2011), and continues with the progression of the disease (Bergsland et al., 2012; Henry et al., 2008; Preziosa et al., 2017; Ramasamy et al., 2009). Thalamic atrophy has also been shown to correlate with cognitive dysfunction (Batista et al., 2012; Bergsland et al., 2016; Bisecco et al., 2017; Houtchens et al., 2007) in MS, which is in line with other studies showing an association between thalamocortical connectivity and diverse functions of higher level cognitive processes (Fama and Sullivan, 2014), including attention, speed of information processing, working memory, and episodic memory processes (Hughes et al., 2012; Philp et al., 2014; Ystad et al., 2010; Ystad et al., 2011).

However, despite its potential direct involvement in cognitive dysfunction, disability, and disease progression, comparatively little is known about the mechanisms of thalamic involvement in MS. One reason for the relative scarcity of mechanistic studies is that the thalamus exhibits similar MR-relevant properties as circumjacent white matter (WM) tissues (Kanowski et al., 2014; Tourdias et al., 2014), like T_1 and T_2 relaxation times and proton density, which hampers *in vivo* investigations with clinical MRI. In particular, the anatomical complexity of the human thalamus, which consists of approximately 100 distinct

cell groups or nuclei (Axer and Niemann, 1994) with distinct connectivity profiles (Fama and Sullivan, 2014; Postuma and Dagher, 2006; Sherman and Guillery, 2013b), has been inaccessible *in vivo* until recently. The increasing availability of higher magnetic field strengths and advanced MRI acquisition and analysis techniques has enabled imaging studies with improved resolution and sensitivity toward new biophysical tissue properties, recently enabling a more detailed *in vivo* assessment of the thalamus (Abosch et al., 2010; Behrens et al., 2003; Bisecco et al., 2015; Unrath et al., 2008; Wiegell et al., 2003). These developments have increased the interest in exploring the involvement of the thalamus in neurological diseases (Minagar et al., 2013).

Quantitative Susceptibility Mapping (QSM) is such a novel advanced MR-based technique (Duyn, 2013; Haacke et al., 2015; Liu et al., 2015; Reichenbach et al., 2015; Schweser et al., 2011; Schweser et al., 2016; Wang and Liu, 2015) that allows for the precise anatomical depiction of intra-thalamic nuclei and even allows quantifying tissue property alterations with high spatial resolution (Deistung et al., 2013) and reproducibility (Deh et al., 2015; Feng et al., 2017; Lin et al., 2015; Santin et al., 2017) at clinically feasible scan times. Various histological validation studies have demonstrated that *magnetic susceptibility*, the quantity provided by QSM, reflects the tissue concentrations of paramagnetic iron complexes (Langkammer et al., 2012; Schenck, 1992; Stüber et al., 2014; Stüber et al., 2016; Zheng et al., 2013) as well as, in an opposite way, myelin (Groeschel et al., 2016; Schweser et al., 2011; Stüber et al., 2014) and calcium (Chen et al., 2014b; Schweser et al., 2010; Straub et al., 2016a; Stüber et al., 2014). Within the MS research, QSM is increasingly being used for the characterization of iron load in the deep gray matter (DGM) (Al-Radaideh et al., 2013; Blazejewska et al., 2015; Hagemeier et al., 2017; Langkammer et al., 2013; Ropele et al., 2017; Rudko et al., 2014; Schmalbrock et al., 2016) and lesions (Bian et al., 2016; Chen et al., 2014a; Cronin et al., 2016; Eskreis-Winkler et al., 2014; Harrison et al., 2016; Kakeda et al., 2015; Li et al., 2016; Wisnieff et al., 2015; Zhang et al., 2016).

In the present study, our central hypothesis was that MS is associated with increased magnetic susceptibility in the thalamus. We further hypothesized that the most substantial differences between patients and controls would be observed in the pulvinar (PUL) nucleus and the lateral nuclear region (LNR) because of potential trans-synaptic degeneration emerging from the motor and visual cortices, regions that are highly affected by MS (Calabrese et al., 2007) and maintain relatively rich structural connectivity with the PUL and LNR. We based our hypothesis on a significant body of literature on DGM iron accumulation in MS (Ropele et al., 2017; Stephenson et al., 2014; Stüber et al., 2016) as well as the well-documented fact that MS leads to demyelination and atrophy. Both the accumulation of iron and loss of myelin increase the tissue's magnetic susceptibility, which leads to a hyper-intense appearance on the susceptibility maps. Furthermore, thalamic atrophy, which occurs early in the course of MS due to demyelination and neurodegeneration, would increase the observed susceptibility simply because of a condensation of the iron present in the tissue.

Several previous MRI studies indicated increased *thalamic* iron in MS (Drayer et al., 1987; Rudko et al., 2014; Zivadinov et al., 2012), such as our previous work with susceptibility-weighted imaging (SWI) MRI, in which PUL was atrophied and signal changes inidcated an

increased susceptibility early in the disease course of pediatric and clinically isolated syndrome (CIS) patients (Hagemeier et al., 2012; Hagemeier et al., 2013b). Further support for our hypothesis was provided by previous studies using positron emission tomography (PET) (Banati et al., 2000; Herranz et al., 2016; Kauzner et al., 2016; Rissanen et al., 2014) and histopathology (Haider et al., 2014; Vercellino et al., 2009) indicating increased microglia activation and influx of highly iron-laden macrophages in the thalami of MS patients, respectively. Also, histopathologic evidence exists for substantial focal demyelination and neuronal loss in the thalamus (Cifelli et al., 2002; Haider et al., 2014; Vercellino et al., 2009). Overall, previous literature strongly argued for a susceptibility increase in the thalamus of MS patients.

To test our hypothesis, we used QSM to examine intra-thalamic alterations of magnetic susceptibility in patients with CIS and MS as compared to matched healthy controls. QSM combines two crucial properties for the study of such a complex structure as the thalamus: first, it delivers high resolution images and enables the depiction of anatomical details that have been inaccessible with other *in vivo* imaging techniques, forming the basis of a volumetry of the thalamic substructures. Second, QSM represents a unique tool to assess the tissue composition via quantitative measurements of the tissue's magnetic susceptibility. We combined volumetry and susceptibility quantification to dissect thalamic iron and myelin mass changes from apparent susceptibility increases that may result from atrophy without actual iron transported into the brain across the blood-brain barrier. A voxel-based analysis (VBA) of the susceptibility maps was applied to reveal disease-related thalamic susceptibility changes without prior assumptions about the location of the changes within the thalamus.

We compared each MS phenotype separately against a dedicated control group that was group matched for age and sex to the different MS/CIS cohort because MS-specific thalamic pathology develops on top of a well-established background of normal aging-related linear atrophy rates (Cherubini et al., 2009; Sullivan et al., 2004), and non-linear tissue iron concentrations. In particular, the latter peaks in the fourth decade of life and decreases thereafter (Bartzokis et al., 2007; Hagemeier et al., 2013a; Hallgren and Sourander, 1958; Mitsumori et al., 2009; Persson et al., 2015), which is difficult to model statistically, complicates the comparison of groups that are not perfectly age-matched, and could affect the comparison of the different clinical phenotypes of MS, including CIS, Relapsing-Remitting (RR) and Secondary Progressive (SP) patients. These disease-subtypes are difficult to match properly on age and typically center on average ages right before, at, and after the characteristic peak of iron concentration in the thalamus, respectively.

2. Subjects and Methods

2.1 Subjects

The study was approved by the local Ethical Standards Committee at the University at Buffalo, and a written informed consent form was obtained from all participants. We enrolled 40 patients in each of the three patient groups (CIS, RRMS, SPMS; 120 patients total) and 40 normal controls (NC) in each of the three control groups (CIS-NC, RRMS-NC, and SPMS-NC; 120 NCs total). The female to male sex ratio was approximately 3, reflecting

the average sex incidence rate ratio of MS in the general population of North America (Trojano et al., 2012). Exclusion criteria were pregnancy and pre-existing medical conditions known to be associated with brain pathology (e.g., cerebrovascular disease or a positive history of alcohol dependence). MS/CIS patients were diagnosed using the revised McDonald criteria (Polman et al., 2011), and clinical disease severity was measured using the Expanded Disability Status Scale (EDSS) (Kurtzke, 1983). Table 1 summarizes the demographics and clinical details of the study groups. Patients with CIS had the lowest EDSS and disease duration, followed by patients with RRMS, and patients with SPMS. The average ages of the three patient groups were significantly different (CIS/RRMS: p=0.004; RRMS/SPMS: p<0.001; CIS/SPMS: p<0.001).

The three groups of each 40 age- and sex-matched normal controls (NC; CIS-NC, RRMS-NC, and SPMS-NC) had a normal neurological examination and no history of neurologic disorders or chronic psychiatric disorders. Neither ages nor sex-ratio of the NC groups were significantly different from the respective patient groups (CIS-NC: age p=0.96, sex p=0.81; RRMS-NC: age p=0.84, sex p=0.46; SPMS-NC: age p=0.79, sex p=1.00). The average ages of the three NC groups were significantly different (CIS-NC/RRMS-NC: p=0.005; RRMS-HC/SPMS-HC: p=0.001; CIS-HC/SPMS-HC: p<0.001).

2.2 MRI

Participants were imaged with a clinical 3T GE Signa Excite HD 12.0 scanner (General Electric, Milwaukee, WI, USA) using an eight-channel head-and-neck coil. Data for QSM were acquired using an unaccelerated 3D single-echo spoiled gradient recalled echo (GRE) sequence with first-order flow compensation in read and slice directions, a matrix of 512×192×64 and a nominal resolution of 0.5×1×2 mm^3 (FOV=256×192×128 mm^3), flip angle = 12°, TE/TR=22ms/40ms, bandwidth=13.89 kHz, and a total measurement time of 8 minutes and 46 seconds (Zivadinov et al., 2012). The anisotropic voxel size resulted from a reduction of the number of phase and slice encoding steps to minimize the total measurement time and, hence, motion artifacts. Because the scanner software did not allow an online reconstruction of phase images for QSM, we saved the raw k-space data for each coil channel. To allow a determination of the total brain volume, we applied an axial high-resolution 3D magnetization prepared T_1-weighted (T1w) fast spoiled gradient-echo pulse sequence with inversion recovery (IR-FSPGR) using the following parameters: TE/TI/TR=2.8ms/900ms/5.9ms, matrix=256×192×128 matrix, nominal resolution of 1×1×1.5mm^3 (FOV=256×192×192mm^3), and flip angle = 10°. No hard- or software upgrades of the MRI system occurred during the duration of the study.

2.3 Data Processing and Analysis

The data processing is schematically illustrated in Figure S.1. The analysts performing the data processing were blinded to the study groups and the scope of the study.

QSM—QSM-related processing was performed by a fully automated pipeline with in-house developed MATLAB programs (2013b, The MathWorks, Natick, MA) on a Linux workstation (Ubuntu 12.04) with 48 cores (Intel Xenon E5-2697v2 at 2.7Ghz) and 396 GB

RAM. Susceptibility maps were reconstructed as described previously (Hagemeier et al., 2017); details are given in the Supplementary Material 1.

Voxel-based analysis (VBA)—For the VBA, susceptibility maps were normalized with the diffeomorphic Greedy-SyN transformation model (Advanced Normalization Tools; version 2.1; http://stnava.github.io/ANTs) to an in-house generated susceptibility brain template with $1mm^3$ isotropic voxel size. The template had been created independently from the present study dataset based on sixty randomly selected susceptibility maps of patients with different diseases and NCs over a wide range of ages using the diffeomorphic Greedy-SyN transformation model with an intensity rescaling strategy (DIR-R) described previously (Hanspach et al., 2017). The template is illustrated in Figure 1.

After smoothing with a 1mm Gaussian kernel, we compared the control groups to one another to determine if previously reported aging-related differences in iron concentrations between the groups could be replicated. Furthermore, we performed a voxel-wise statistical analysis via non-parametric permutation tests (FSL randomise (Winkler et al., 2014); 5000 permutations) using age and sex as covariates to identify susceptibility differences between patient groups and their respective control groups. Threshold-free cluster enhancement (TFCE) while controlling for family-wise error (FWE) rate revealed significant differences between groups at the level of $p<0.05$. Given the study objectives, we restricted the statistical analysis to voxels within the thalamus, which also increased the statistical power. The procedure used to define this region is described below.

Atlas-based analysis—To gain insight into volume changes of thalamic subnuclei and to quantify susceptibility differences between groups, we applied an atlas approach. Toward this end, we created a custom thalamic nuclear atlas by identifying and outlining clearly identifiable thalamic substructures on the susceptibility brain template with Freeview (FreeSurfer 5.3.0, Athinoula A. Martinos Center for Biomedical Imaging, Charlestown, MA). The atlas was created slice-by-slice by a trained image analyst (A.L.R.D.M.; 2 years of experience in neuroimaging) in consultation and based on consensus with an expert in brain susceptibility contrast (F.S.; 9 years of experience in neuroimaging). Identification of substructures was facilitated by a direct comparison of the template with cytoarchitectonic plates of the thalamus in the Schaltenbrand and Wahren atlas (Schaltenbrand et al., 1977), which has been shown to be the most suitable atlas for a segmentation of *in vivo* MR images (Deistung et al., 2013; Kanowski et al., 2014). Anatomical regions that appeared as a contiguous structure on the susceptibility template and could not be sub-segmented were treated as a single structure in the atlas, even if cytoarchitectonic plates and ultra-high field QSM (Deistung et al., 2013) suggested subdivisions. In addition to thalamic subnuclei, we outlined the thalamus as a whole (global thalamus; GT) to facilitate a comparison with previous studies.

We transformed the atlas to the original susceptibility maps with nearest neighbor interpolation by applying to the atlas the inverse of the non-linear transformations to the template space. We calculated the volume of each region of the warped susceptibility atlas and normalized it to the head volume, as determined by FMRIB's SIENAX cross-sectional software tool (version 2.6) (Smith et al., 2002).

Statistical analysis of regional average values of volume and susceptibility— The statistical analysis of regional average values was performed using the Statistical Package for the Social Sciences (SPSS; version 24; IBM, Armonk, NY) and Excel (version 1701; Microsoft, Redmond, WA). All sample distributions were tested for normality using the Shapiro-Wilk test and visual examination of Q-Q-plots. If distributions were normal, paired *t*-tests were used to determine whether mean values differed between left and right hemispheres for each anatomical region. If distributions were non-normal, we used the Wilcoxon signed rank test. If a significant inter-hemispheric difference was found in either the patient group or the respective control group, further analyses of the structure were carried out for both hemispheres separately; otherwise, further analyses used the mean of left and right hemisphere values. Univariate ANCOVA with sex as a covariate was applied to determine if mean values of controls and patients differed significantly from one another.

We have previously estimated that increased *caudatal* susceptibility observed in MS may be driven by a loss of tissue compartments with little iron (Hagemeier et al., 2017). To understand if this effect could also be the driving force leading to increased PUL susceptibility, we calculated the Pearson correlation coefficients for volume and susceptibility. For simplicity, this correlation analysis was performed for bi-hemispheric average values. To investigate the presumably nonlinear effect of normal aging on thalamic susceptibility and volume, we calculated the Spearman rank correlation coefficients for susceptibility and volume, respectively, using all 120 subjects of the three NC groups.

Effect sizes were estimated using Cohen's *d*. Statistical significance levels were corrected for FWE rate using the Bonferroni procedure. Findings with $p \leq 0.05$ that did not reach statistical significance after the correction are reported as "trends" to counter-balance the conservative nature of the multiple comparison corrections.

To characterize the relative effects of age, disease duration (dd), and sex on the observed variables, we performed a multiple regression analysis. Variable transformations were performed if histograms and scatterplots indicated they were necessary. Since results from multivariate analyses with transformed variables are difficult to interpret, we repeated all analyses with untransformed variables. Reliability of fitting coefficients was determined by performing a collinearity analysis with a condition index threshold of 15 and variance proportions exceeding 90 in two or more variables.

3. Results

We report anatomical locations within the thalamus according to the recommendations of the Federative Committee on Anatomical Terminology (Federal Committee on Anatomical Terminology, 1998) and use neurological display convention in all figures (subject's left is shown on the left).

Voxel-based analysis

Susceptibility differences between the three NC groups, CIS-NC, RRMS-NC, and SPMS-NC, did not reach statistical significance (F-test). For demonstrative purposes, we calculated the group differences and Z-score maps of the control groups, which may be found in

Supplementary Figure S.2. While some nuclear groups could be discerned on these maps, group-average difference maps had a noisy appearance, and Z-scores did not exceed 0.5.

Figures 2a and S.3 show the regions of significant susceptibility differences between patients and controls after Threshold-Free Cluster Enhancement (TFCE). Figures 2b and S.4 show the corresponding group-average difference maps and Z-score maps. While the comparison of CIS patients with CIS-NCs did not reach statistical significance, it indicated a relatively localized disease-related susceptibility *increase* in the PUL and susceptibility *decrease* in the remaining part of the thalamus, Z-scores were low overall.

RRMS patients showed a statistically significant susceptibility reduction compared to RRMS-NCs, which reached statistical significance primarily in the left thalamus, whereas the right thalamus was largely unaffected apart from a small region with susceptibility reduction located in the central medial intralaminar nucleus of the thalamus (arrow I in Fig. 2a and S.3; between the medial dorsal nucleus and the anterior nuclei of the thalamus). The reduced susceptibility in the left hemisphere was localized in the medial dorsal nucleus (arrow II) and the ventral posterolateral nucleus (also *nuclei ventrocaudales*; arrow III). Reduced susceptibility was also observed bilaterally in a small region localized at the medial pulvinar (PUL; arrow IV; see (Stepniewska, 2004) for PUL subdivisions).

In SPMS, we found susceptibility reductions compared to SPMS-NCs that were more symmetric than in the RRMS group. In particular, significantly reduced susceptibility was found bilaterally in the medial dorsal nucleus (arrow II) and the PUL (arrow V). While the whole PUL was affected in the left hemisphere, changes in the lateral division of the medial PUL (arrow VI) in the right hemisphere did not reach statistical significance. A comparison with the group difference maps and Z-scores indicated that both PULs were homogeneously affected and the lack of statistical significance was due to a higher variability between subjects in the center of the PUL (Fig. S.4). Contrary to the RRMS group, we did not find significant differences in the ventral posterolateral nucleus.

Altas-based analysis

Comparison of the susceptibility brain template with the Schaltenbrand and Wahren atlas (Schaltenbrand et al., 1977) led to the unambiguous identification of the following three major nuclear regions of the thalamus: PUL, medial nuclei region (MNR), and lateral nuclei region (LNR). The anterior nucleus appeared hyper-intense but blended over into the cerebrospinal fluid, rendering a reliable segmentation difficult. A further parcellation of the nuclear groups, as reported in previous ultra-high field work (Deistung et al., 2013), was not possible. Figure 1 illustrates the anatomical locations of the identified regions.

The average susceptibilities and volumes in the patient and control groups are listed in Tabs. 2 and 3, respectively. The PUL showed the highest average magnetic susceptibility among all regions, in line with earlier QSM-based work (Deistung et al., 2013) and iron stains showing the strongest reactivity in this region (Morris et al., 1992; Spatz, 1922). Although both LNR and anterior nucleus had been described among the regions with the strongest iron reactivity (Morris et al., 1992), the LNR appeared less paramagnetic than the anterior nucleus (data not shown) and the MNR. This observation may be explained by the relatively

high myelin content of the LNR compared to other thalamic regions (Schaltenbrand et al., 1977), which counteracts the effect of iron on the voxel susceptibility.

Group differences—The distributions of susceptibilities and volumes were normal in all groups and regions except for the PUL volumes in SPMS. Consistent with the VBA-results, differences between CIS and CIS-NCs did not reach statistical significance ($p \geq 0.11$; $|d| \leq 0.36$). In RRMS patients, we found statistically significant reductions of susceptibility compared to RRMS-NCs in the GT (−5.9 ppb; $d=-0.86$; $p<0.001$) and, consistent with the VBA, in the left MNR (−9.7 ppb; $d=-0.84$; $p<0.001$) and left LNR (−5.1 ppb; $d=-0.75$; $p=0.001$). Trends toward lower susceptibility in patients were observed in the PUL (−5.3 ppb; $d=-0.50$; $p=0.028$) and in the right MNR (−7.8 ppb; $d=-0.57$; $p=0.019$). In SPMS patients, magnetic susceptibility was significantly reduced compared to SPMS-NCs in all regions (≤−7.0 ppb; $d \leq -1.18$) except in the LNR ($d=-0.44$; $p=0.051$), in line with the VBA findings.

Volume differences between CIS and CIS-NCs did not reach statistical significance, but disease-related atrophy was indicated by trends in the right GT (−0.28 ml; $d=-0.47$; $p=0.043$) and the right PUL (−0.15 ml; $d=-0.49$; $p=0.034$). In both RRMS and SPMS patients, volume reductions relative to the individual NC groups reached statistical significance in all regions (except for a trend in the right MNR of RRMS). Effect sizes were $|d| \geq 1.0$ in all areas except the MNR ($|d| \geq 0.6$).

Associations between susceptibility and atrophy—Table 4 lists the correlations of susceptibility and volume for all groups. Correlations were *positive* in all regions. Statistical significance was reached in the PUL of all patient groups ($r>0.399$, $p<0.011$), the PUL of SPMS-NCs ($r=0.414$, $p=0.008$), and the MNR of RRMS-NCs ($r=0.508$, $p<0.001$) and SPMS-NCs ($r=0.525$, $p=0.001$). Trends were observed in PUL (CIS-NC and RRMS-NC), MNR (all patient groups), and GT (all patient groups and SPMS-NC).

Multivariate linear regression—A histogram analysis revealed a positively skewed distribution of the dd, which could be mitigated by a log-transform of the variable. Scatterplots correlating susceptibility with age and dd, respectively, indicated non-linear associations of susceptibility with age in the PUL and with the log-transformed dd in PUL and MNR, which could be described by a quadratic relationship. A similar analysis for the volumes revealed non-linear associations of left/right PUL with transformed dd and LNR with age and transformed dd. Hence, we performed a multivariate regression analysis with susceptibility and volume as dependent outcomes, respectively, and the following transformed independent variables in all 120 patients: age^2 [susceptibility: PUL; volume: LNR], ln(dd) [susceptibility: GT, LNR; volume: all], and $\ln(dd)^2$ [susceptibility: PUL, MNR; volume: PUL, LNR], respectively.

We found significant negative associations of right GT susceptibility with ln(dd) [$p<0.001$, partial correlation $R_p=-0.34$], average PUL susceptibility with $\ln(dd)^2$ [$p<0.001$, $R_p=-0.42$], and left MNR susceptibility with age [$p=0.004$, $R_p=-0.28$]. Trends toward negative associations were found for the left GT susceptibility with ln(dd) [$p=0.029$, $R_p=-0.21$] and age [$p=0.035$, $R_p=-0.21$], for the right MNR susceptibility with $\ln(dd)^2$ [$p=0.017$, $R_p=$

−0.23], and for the left LNR susceptibility with age [p=0.028, R_p=−0.21]. For volumes, we found significant negative associations between right GT and ln(dd) [p<0.001, R_p=−0.33], PUL and ln(dd)^2 [p<0.001, R_p=−0.32/−0.38], left MNR and age [p<0.001, R_p=−0.34], and LNR and ln(dd)^2 [p<0.001, R_p=−0.35]. Trends were found for negative associations of left GT with age [p=0.012, R_p=−0.24] and ln(dd) [p=0.045, R_p=−0.20] and right MNR with ln(dd) [p=0.019, R_p=−0.23]. Associations with sex did not reach p≤0.05 in any of the regions.

Age (and age^2) correlated significantly with ln(dd) [and ln(dd)^2] (Pearson 0.63≥R≥0.61, p<0.001), but condition indices of the collinearity analyses between the variables did not exceed 14 in any of the analyses. Supplementary Material 2 summarizes the results of the multivariate analyses with untransformed variables for susceptibility and volumes, respectively. The directions of the dependencies were largely in line with the analyses using transformed variables. Statistically significant univariate correlations are plotted in Figure 3.

4. Discussion

13 This work is the first systematic assessment of intra-thalamic susceptibility variations across the clinical spectrum of MS. We found significantly reduced magnetic susceptibility in specific thalamic subregions of patients with RRMS and SPMS, in particular in the PUL, but not in patients with CIS. Susceptibility reduction was significantly associated with increase in dd. In the following, we discuss our findings in the light of previous works and provide a mechanistic interpretation. In particular, we believe that the integrative role of the thalamus in brain function and the common notion of iron *increase* as a driver in neurodegeneration justify a detailed discussion of the potential biophysical origin and mechanistic processes underlying our findings.

Previous susceptibility-based MRI studies in MS that are consistent with our findings

In CIS patients, we found increased susceptibility in the PUL (Figure 2b), but group differences did not reach statistical significance (d=0.14; Tab. 2). This finding is (partially) in line with previous studies by Al-Radaideh et al. (Al-Radaideh et al., 2013), Langkammer et al. (Langkammer et al., 2013) and Elkady et al. (Elkady et al., 2017), which did not find statistically significant changes in the thalamus of CIS patients with QSM, and previous studies by our group reporting significantly *increased* iron load in the PUL of CIS patients (Hagemeier et al., 2012; Zivadinov et al., 2012) using a predecessor techniques of QSM. Although statistically insignificant, the group differences between CIS patients and controls found by Elkady et al. (Elkady et al., 2017) (Fig. 3a in that publication) closely resembled our findings of increased susceptibility in the PUL and decreased susceptibility in the rest of the thalamus (Fig. 2b).

In RRMS patients, we found significantly decreased GT susceptibility. This finding is consistent with recent QSM-based studies by Burgetova et al. (Burgetova et al., 2017) (−3.3ppb, p=0.004) and by our group (Hagemeier et al., 2017) (−5.7ppb, d=0.71–0.94, p<0.001). Also similar to the present work, Burgetova et al. observed reduced thalamic susceptibility in RRMS only when excluding the PUL and not in the PUL itself. This

observation is consistent with group differences shown by Elkady et al. (Elkady et al., 2017) (Fig. 3b in that publication).

Previous susceptibility-based MRI studies in MS that are inconsistent with our findings

Several authors did not find significant GT changes in patients with RRMS (or mixed phenotype groups) using either QSM (Elkady et al., 2017; Fujiwara et al., 2017), the effective transverse relaxation rate (R_2*) (Fujiwara et al., 2017), or different iron-sensitive non-QSM techniques (Du et al., 2015; Hagemeier et al., 2013b; Raz et al., 2014). Other studies suggested *increased* GT iron in RRMS with QSM (Cobzas et al., 2015) and other techniques (Cobzas et al., 2015; Ge et al., 2007; Modica et al., 2014). Rudko et al. (Rudko et al., 2014) reported increased susceptibility relative to controls in a mixed group of CIS and RRMS patients, but differences in R_2* between CIS and RRMS patients of similar age did not reach significance (Khalil et al., 2009).

In the present study, the PUL appeared unaltered in RRMS patients and showed significantly decreased values in SPMS when compared to NCs. In line with previous work (Henry et al., 2008), we found both atrophy and reduced susceptibility in the left MNR of our RRMS group and bilaterally in SPMS patients. However, we could not confirm the previous findings of significant atrophy of the bilateral MNR and bilateral PUL in CIS (Henry et al., 2008). Inconsistent with the present study is also the *increased* PUL iron load that has been suggested in RRMS using QSM (Al-Radaideh et al., 2013; Elkady et al., 2017; Rudko et al., 2014), R_2* (Elkady et al., 2017; Lebel et al., 2012; Quinn et al., 2014; Walsh et al., 2014), and other techniques (Haacke et al., 2010; Habib et al., 2012; Hagemeier et al., 2013b; Modica et al., 2014; Zivadinov et al., 2012; Zivadinov et al., 2010).

Heterogeneity of the literature on brain-iron in MS—Overall, the literature is highly heterogeneous with respect to the outcomes of brain iron studies in MS. This observation may be explained by the wide variety of techniques employed for imaging, reconstruction, and analysis. Even a direct quantitative comparison between studies that employed QSM is difficult because the studies employed different reference regions (or did not specify the region used), phase processing techniques (Özbay et al., 2017; Schweser et al., 2017b), and QSM algorithms (Wang and Liu, 2015). A comparison with non-QSM techniques, such as R_2* mapping, is even more problematic because of confounding sensitivities on the microdistribution and chemical form of iron (Dietrich et al., 2017) as well as the microstructure. Furthermore, the non-linear aging trajectory of the thalamic iron concentration (Hallgren and Sourander, 1958) and the heterogeneity of the disease render a comparison of groups with different clinical and demographic characteristics challenging. An overview of the substantial differences between the cohorts studied in the literature may be found in the Inline Supplementary Tab. S.3. Interestingly, Burgetova et al.'s study, which is largely consistent with the present work, relied on a cohort relatively similar to our RRMS group.

The comparison of the group characteristics and outcomes of published studies led us to the proposal of a *early-rise late-decline hypothesis*: Increased PUL susceptibility may be found predominantly in younger patients with an average age below 40 years (all studies published

before 2017; cf. Tab. S.3), whereas in older patients, such as those studied in the present and in our previous work (Hagemeier et al., 2017), PUL susceptibility in patients was, on average, lower than in controls. The observed significant reduction of PUL susceptibility with dd ($p<0.001$) further supports this hypothesis. Moreover, in a recent R_2*-based follow-up study, Khalil et al. (Khalil et al., 2015) suggested that not only in the thalamus but also in other brain regions iron accumulation is more pronounced in the early stages than in the later stages of the disease. Showing that iron decreases over time already in CIS, this study also suggests that peak iron concentration may be observed (best) *before* the first clinical symptoms. However, since the authors did not enroll a control group, it remained unclear if the observed temporal iron decrease exceeded the normal aging-related iron decrease. Hence, the authors' conclusion, although consistent with our findings, warrants further investigation.

Biophysical explanation of the observed thalamic susceptibility alterations

A decrease of magnetic susceptibility toward more diamagnetic values can be explained by both a reduction of the contributions from paramagnetic compounds (such as ferritin-bound iron) and an increase in the contributions from diamagnetic compounds (such as myelin or calcium); a change toward higher susceptibility values vice versa. While calcium may play a role in MS (see Supplementary Material 3 for a detailed discussion), no strong evidence exists for a substantial calcium accumulation in the thalamus. Hints on the underlying biophysical mechanisms of the observed susceptibility decrease may be obtained from correlations of susceptibility and R_2*. The two measures have a similar dependence on paramagnetic but an opposite dependence on diamagnetic tissue compartments; iron increases both of them, whereas calcium decreases/increases susceptibility/R_2*. Hence, thalamic susceptibility and R_2* values would be expected to correlate *negatively* if calcium had a significant contribution to the variations between observed measures. Fujiwara et al. (Fujiwara et al., 2017) recently performed such a partial correlation analysis correcting for age and sex in the DGM of MS patients. However, they reported a significant *positive* correlation in the thalamus ($r=0.6$; $p<0.001$) as well as all other DGM. This observation indicates that variations in the tissue concentration of iron, but not calcium, dominate the inter-subject variations of susceptibility and R_2* in MS. Interestingly, the authors found significant positive correlations also in the DGM of NCs, but not in their thalami ($r=0.03$; $p=0.89$). This discrepancy between MS patients and NCs may be explained by the relatively high amount of diamagnetic myelin in the thalamus of NCs, which counteracts the positive correlation, and the reduced amount of myelin in MS.

The most plausible explanation of *increased* PUL magnetic susceptibility early in the disease (Fig. 2b and previous work) is the iron accumulation of microglia (Banati et al., 2000; Haider et al., 2014; Herranz et al., 2016; Kauzner et al., 2016; Rissanen et al., 2014). Recent evidence for a chronic intravascular haemolysis (Lewin et al., 2016) and a correlation of serum iron with DGM susceptibility changes (Bergsland et al., 2017) in MS point toward a translocation of blood-iron into the brain, where it accumulates in microglia, a process that has been hypothesized already by Metz and Spatz in 1924 (Metz and Spatz, 1924). DGM may be particularly prone to the inlux of heme-iron due to their high perfusion compared to WM. In principle, also the reduction of the relative voxel volume fraction of myelin

associated with the focal thalamic demyelination in MS (Haider et al., 2014; Vercellino et al., 2009) could increase the susceptibility. However, while the thalamus is higher myelinated than other DGM regions, myelin stains show that the PUL is one of the regions with the least amount of myelin in the thalamus (Schaltenbrand et al., 1977), rendering it unlikely that demyelination in this region explains a substantial increase of the tissue susceptibility.

The decrease of magnetic susceptibility in later stages of the disease most likely involves iron-containing thalamic cells. In both WM and DGM of normal brain, most of the iron is found in oligodendrocytes and their processes (Bagnato et al., 2011; Francois et al., 1981; Haider et al., 2014; Hill and Switzer III, 1984; Meguro et al., 2008). Iron-staining in rats indicated a higher number of iron-laden oligodendrocytes as well as a higher iron load of individual oligodendrocytes in the DGM than in the WM (Meguro et al., 2008). In human DGM, approximately 30% of the cell bodies have been reported to be oligodendrocytes (in the caudate) (Myers et al., 1991b), most of them are probably perineuronal satellite oligodendrocytes with unknown functions (Verkhratsky, 2013). Hence, the substantial *reduction* of the magnetic susceptibility below that in NCs, as observed in definite MS (Tab. 2 and Fig. 2b), points toward a decrease of the oligodendrocyte density or a depletion of iron from oligodendrocytes. In fact, using diaminobenzidine (DAB)-enhanced Turnbull blue staining for ferrous and ferric iron, Hametner et al. (Hametner et al., 2013) reported a decrease in the iron concentrations in both the WM close to the neocortex (including the iron-rich U-fibers, personal communication) and in the deep normal appearing WM (NAWM; sampled from the whole telencephalon, personal communication) of MS tissue specimens *relative* to that in specimens of NCs. Similar to our findings in the thalamus, the reduction of WM iron correlated significantly with the dd (R^2=0.31, p<0.001). Furthermore, the authors reported a loss of oligodendrocytes and a reduction of non-heme iron within oligodendrocytes and myelin in NAWM. Using ionised calcium-binding adapter molecule 1 (IBA-1) immunoreactivity, the same group later demonstrated a shift of iron from oligodendrocytes to microglia *in the DGM* (Haider et al., 2014). While the authors assessed iron by semi-quantitative densitometry, which may not represent iron concentration linearly, Popescu et al. (Popescu et al., 2017) recently confirmed the decrease of iron with age and disease duration in NAWM of MS patients using X-ray fluorescence imaging, which is an element-specific and quantitative technique. Reduced iron has also been reported in inactive cortical MS lesions (Yao et al., 2014), i.e. lesions with sparse inflammatory cells.

Mechanistic interpretation of the observed thalamic susceptibility alterations

Due to their high oligodendrocyte density, the DGM may be subject to similar pathological processes as the WM. In particular, both NAWM (Frischer et al., 2009) and DGM (Herranz et al., 2016) show chronic microglial activation in MS, with the highest activity in the thalamus (Banati et al., 2000; Herranz et al., 2016; Kauzner et al., 2016; Rissanen et al., 2014). The pro-inflammatory cytokines TNF-α and interferon-γ, expressed by microglia upon activation, have an iron-mediated toxic effect on oligodendrocytes (Zhang et al., 2005) and trigger a *release* of iron from the cells (Zhang et al., 2006). While protective against the direct toxicity of cytokines, this oligodendroglial iron release may itself have several detrimental consequences. First, before the liberated iron is detoxified and cleared from the

region, it might directly contribute to mitochondrial dysfunction and neurotoxicity by fueling the creation of reactive oxygen and nitrogen species via Fenton chemistry. Second, iron deficiency negatively affects several pathways of normal oligodendrocyte function (Connor and Menzies, 1996), the proliferation of oligodendrocyte progenitor cells (Schonberg et al., 2012), their differentiation, and remyelination (Stephenson et al., 2014). Third, microglia that pick up the iron increase the release of proinflammatory cytokines and switch from a quiescent to a pro-inflammatory phenotype (Zhang et al., 2006), further fueling the release of iron from oligodendrocytes in a vicious circle.

The observed *positive* correlation between structural volumes and magnetic susceptibility observed in the present study (Tab. 4) points toward an association between iron depletion and the relatively high number of focal demyelinating lesions previously observed in the thalamus (Haider et al., 2014; Vercellino et al., 2009). This association might result from a loss of iron-containing oligodendrocytes secondary to the lesion formation or be related to a retraction of oligodendrocyte processes under an iron-depletion related stress condition (Rone et al., 2016). Hence, it may be speculated that the bystander damage of chronic inflammation and, in particular, its effect on the local availability of storage iron, represents the missing link between inflammatory and neurodegenerative disease components in MS, partially explaining the slow transition from RRMS to SPMS. In this context, it is an interesting observation that thalamic T_2-hypointensity, indicative of high iron load, predicts the progression of brain atrophy over 1 year in *untreated* MS patients, whereas this relationship diminishes upon immune-modulating treatment with interferon β-1 (Bermel et al., 2005) despite no measurable effect of the drug on the atrophy rate during this time.

An association between chronic microglial activation and iron depletion would provide the missing link also for a mechanistic explanation for the peculiar *normal* aging trajectory of thalamic iron (Fig. S.6). Microglial activation is a poorly understood phenomenon of normal aging, which shows the strongest correlation with age in the thalamus (Schuitemaker et al., 2012).

What distinguishes the thalamus from other brain regions that show predominantly increased magnetic susceptibility in MS?

Strong evidence exists for the common notion that MS is associated with an increase in the DGM iron concentration. This evidence may give rise to the question why the WM and the thalamus show the opposite behavior. However, increased iron concentration, such as that observed in the DGM, does not necessarily imply iron *deposition*. We have estimated in a recent longitudinal QSM-based MS study that the expected increase of caudatal susceptibility due to demyelination and atrophy of cells with little or no iron, *exceeds* the observed susceptibility increase (Hagemeier et al., 2017). In other words, the removal of iron-containing cells or depletion of iron from cells on top of the major demyelination is required to explain the observed longitudinal *increase* of magnetic susceptibility in the caudate of MS patients. This estimation was recently supported by independent preliminary data on total iron estimated from R_2* and volumetric measurements, which indicated decreased total iron in the caudate, pallidum, and thalamus of MS patients (Hernández-Torres et al., 2017). Reduced DGM iron has also previously been observed in other

neurological diseases (Doring et al., 2016; Kanaan et al., 2017). In summary, the depletion of iron may not be restricted to the thalamus but may instead be a general hallmark of MS.

However, its rich connectivity profile and central role in several brain networks might render the thalamus particularly susceptible to secondary effects from remote injury in other parts of the brain via Wallerian degeneration or hypometabolism. This hypothesis is supported by studies showing that the reduction of thalamic NAA in MS (Cifelli et al., 2002; Wylezinska et al., 2003), indicative of neurodegeneration, is correlated with NAA in the frontal NAWM (Wylezinska et al., 2003), and thalamic atrophy and hypometabolism are correlated with WM lesion volume (Blinkenberg et al., 2000; Houtchens et al., 2007). Furthermore, a study by Henry et al. (Henry et al., 2009) suggested a mechanistic relationship between thalamic atrophy and WM lesions in thalamocortical tracts. A recent study in the experimental autoimmune encephalomyelitis (EAE) mouse model for MS reported chronic inflammation and demyelination of the spinothalamic tract at the level of the spinal cord paired with neuronal loss in the thalamic target region of the tract (Wagenknecht et al., 2016). The absence of indicators for autoimmune attack of the thalamus during the acute stage of the disease suggested that the observed thalamic neurodegeneration was secondary to the autoimmune attack in the spinal cord.

It is also known that neuroinflammatory responses can be ‘projected’ bidirectionally along cortico-thalamic tracts (Banati, 2002), where cortical injury induces a remote microglial response in the ipsilateral thalamus (Banati et al., 2001; Kuchcinski et al., 2017; Myers et al., 1991a; Pappata et al., 2000; Sørensen et al., 1996). Consequently, the widespread cortical pathology in MS (Calabrese et al., 2007; Kutzelnigg and Lassmann, 2005), including chronic active lesions with microglial activation (Pitt et al., 2010) and meningeal inflammation (Howell et al., 2011; Kutzelnigg et al., 2005), may spread along cortico-thalamic tracks and, as such, “focus” in the thalamus. In fact, thalamic [11C]-PBR28 binding correlates with cortical thinning and reduced cognitive performance (Herranz et al., 2016).

Remote cortical injury as a driving factor for the observed susceptibility reduction is also supported by the fact that the PUL was the most affected region in the present work. Being the largest of the “association” nuclei (Shipp, 2003), the PUL receives the majority of its input directly from the cerebral cortex and participates primarily in reciprocal cortico-corical interactions. In addition, also the MNR, including the mediodorsal nucleus, is primarily associative, whereas the LNR, which showed only little alteration in the present study, consists of “relay” nuclei, which receive input from the periphery and only forward it to the cortex (Jones, 1991).

It is likely that the strong susceptibility decrease in the PUL observed in the present study is secondary to injury elsewhere in the optical pathways. Cortico-pulvinar-cortical circuitry has an active participation in the processing of visual information and selective attention through the promotion of synchronized activity in different cortical areas (Benarroch, 2015; Fama and Sullivan, 2014). Early studies in monkeys have demonstrated that lesions in the visual cortex (Mathers, 1972; Ogren and Hendrickson, 1979) cause degenerative changes in the PUL. Visual impairment is a frequent symptom of MS and both retinal nerve fiber layer

thickness, and retinal periphlebitis have been associated with disease activity in MS (Sepulcre et al., 2007). More recently, Mühlau et al. (Muhlau et al., 2013) found that WM lesions and PUL atrophy are spatially related in MS, with axonal transection within WM lesions and subsequent degeneration along the axonal projections being the most plausible explanation. Gabilondo et al. (Gabilondo et al., 2014) showed retro- and anterograde trans-synaptic neuronal degeneration in the visual pathway and Zivadinov et al. (Zivadinov et al., 2014) reported a trend toward associations between retinal nerve fiber layer thickness in RRMS patients and microstructural damage in the thalamus, in particular, volume changes in the GT and PUL.

Interestingly, thalamic lesions in MS have previously been reported primarily in the MNR and the anterior nuclear region, but not in the LNR (Vercellino et al., 2009). These observations are in line with the locations of significant susceptibility reduction in our VBA (Figs. 2a and S.3). Several studies have shown that the LNR connects to premotor areas (anterior portion) (Behrens et al., 2003; Bisecco et al., 2015; Johansen-Berg et al., 2005), M1, and somatosensory cortices S1/S2 (posterior portion) (Behrens et al., 2003; Johansen-Berg et al., 2005). The intra-thalamic spatial patterns of regions with thalamo-occipital, -temporal, and -somatosensory projections shown in these publications resemble surprisingly well our QSM-based findings in RRMS, and areas with thalmo-occipital, -parietal, and -frontal projections those in SPMS (Figs. 2a and S.3). Also a recent R_2*-based study in stroke patients (Kuchcinski et al., 2017) reported increased iron in the MNR and PUL following infarcts in more anterior brain regions and more posterior regions, respectively. This selective involvement of areas with specific connectivity profiles further supports a direct relationship between thalamus pathology and pathology in the cortex.

Laterality of susceptibility changes

We observed strong laterality in some regions. Although the reason for the laterality remains unclear, it is not an unexpected finding. Cobzas et al. (Cobzas et al., 2015) reported left-right asymmetry of the p-values in their VBA of thalamus susceptibility. Asymmetry of deep brain regions has also recently been shown in a large multi-center study. In particular, thalamus was among the structures with the highest inter-hemispheric asymmetry (Guadalupe et al., 2016). A meta-analysis by Lansley et al. (Lansley et al., 2013) showed increased atrophy of the left thalamus in patients with RRMS and Preziosa et al. (Preziosa et al., 2017) recently reported a stronger association of atrophy in the left than in the right thalamus with worsening disability and cognitive deterioration over 5 years.

Limitations of the study

Our work has conceptual and technical limitations. Conceptual limitations of the study include the lack of a detailed assessment of the disability profile in patients and its correlation with the intra-thalamic susceptibility changes. It is likely that a link exists between the alterations in sub-nuclei and functional, emotional, and cognitive dysfunction primarily associated with these regions and basal ganglia-thalamocortical pathways. In particular, the globus pallidus is the major input region to the thalamus (Alexander et al., 1986) and, at the same time, one of the DGM regions that show the greatest susceptibility increase in MS (Hagemeier et al., 2017).

To investigate if our findings are strongly associated with clinical disability, we performed an exploratory *post hoc* analysis in which we added EDSS to the multivariate regression analysis (log-transformed due to platykurtic distribution). We observed a statistically significant positive association between the transformed disability and susceptibility in the left (p=0.034) and right (p=0.025) LNR. In all other regions, associations between disability and susceptibility did not reach significance (p>0.05). In particular, we failed to confirm the negative association of the global thalamus susceptibility with EDSS scores previously reported by Burgetova et al. (Burgetova et al., 2017). Considering that the LNR is a region that contains primarily relay nuclei, which forward information from the periphery to the cortex, a more direct association of the LNR with EDSS scores (compared to the association nuclei) seems plausible. A more detailed investigation of the associations of susceptibility alterations in thalamic sub-nuclei with clinical disability will be the subject of future research.

Another limitation of our study is that we could not demonstrate that thalamic susceptibility explains more variance than other, more conventional MRI measures and did not take into account the thalamic lesion burden. In addition, although the design of our cross-sectional study controlled for confounding effects to the extent possible, longitudinal studies are needed to control for cohort effects that affect the whole cohort equally.

We discuss the technical limitations of the study in the Supplementary Material 4.

Conclusion

In conclusion, the results of the present study falsified our hypothesis of increased thalamic susceptibility. Our findings suggest that thalamic susceptibility decreases with dd and that thalamic sub-regions follow distinct temporal trajectories. The inconsistency of this result with some previous studies may be attributed to a substantial heterogeneity of clinical characteristics, imaging methods, and group demographics, particularly a lower group-average age in previous studies. Although the biophysical origin of the decreased thalamic susceptibility remains unclear, a plausible explanation that is supported by independent previous work is the depletion of iron from oligodendrocytes, which may be a side effect related to chronic microglia activation and ultimately lead to neurodegeneration. Because the different thalamic nuclei maintain distinct connectivity profiles that form a closely coupled system with virtually all cortical and subcortical areas (Fama and Sullivan, 2014; Postuma and Dagher, 2006; Sherman and Guillery, 2013b), the observed pathologic alterations in thalamic tissue properties may have wide-spread interaction effects with other disease mechanisms and symptoms in MS.

Supplementary Material

Refer to Web version on PubMed Central for supplementary material.

Acknowledgments

We are grateful to Dejan Jakimovski (University at Buffalo, BNAC) for the thorough reading of our manuscript and his valuable comments and suggestions, Dr. Gregory Wilding (University at Buffalo; Biostatistics, Epidemiology

and Research Design (BERD) Core) for valuable advice regarding the statistical analyses, and Devika Rattan (University at Buffalo; Buffalo Neuroimaging Analysis Center) for support with the image analysis.

Funding

Research reported in this publication was funded by the National Center for Advancing Translational Sciences of the National Institutes of Health under Award Number UL1TR001412. The content is solely the responsibility of the authors and does not necessarily represent the official views of the NIH.

Abbreviations

Avg	Average
CI	Confidence Interval
CIS	Clinically Isolated Syndrome
DAB	Diaminobenzidine
dd	Disease Duration
DGM	Deep Gray Matter
EDSS	Expanded Disability Status Scale
FOV	Field of view
FWE	Family-Wise Error
GRE	Gradient Recalled Echo
GT	Global Thalamus
IBA-1	Ionised Calcium-Binding Adapter Molecule 1
IQR	Interquartile Range
IR-FSPGR	Fast Spoiled Gradient-Echo Pulse Sequence With Inversion Recovery
LNR	Lateral Nuclear Region
MNR	Medial Nuclear Region
MS	Multiple Sclerosis
NAWM	Normal Appearing White Matter
NC	Normal Controls
PET	Positron Emission Tomography
ppb	Parts Per Billion
PUL	Pulvinar
QSM	Quantitative Susceptibility Mapping
R_2*	Effective Transverse Relaxation Rate

RRMS	Relapsing-Remitting MS
SPMS	Secondary Progressive MS
SWI	Susceptibility-Weighted Imaging
T_1w	T_1-Weighted
TFCE	Threshold-Free Cluster Enhancement
WM	White Matter

References

Abdul-Rahman HS, Gdeisat MA, Burton DR, Lalor MJ, Lilley F, Moore CJ. Fast and robust three-dimensional best path phase unwrapping algorithm. Appl Opt. Sep; 2007 46(26):6623–35. http://www.ncbi.nlm.nih.gov/pubmed/17846656. [PubMed: 17846656]

Abosch A, Yacoub E, UÄŸurbil K, Harel N. An assessment of current brain targets for deep brain stimulation surgery with susceptibility-weighted imaging at 7 tesla. Neurosurgery. Dec; 2010 67(6): 1745–56. discussion 1756. http://-www.pubmedcentral.nih.gov/-articlerender.fcgi?artid=3124849&tool=pmcentrez&rendertype=abstract. [PubMed: 21107206]

Al-Radaideh AM, Wharton SJ, Lim SY, Tench CR, Morgan PS, Bowtell RW, Constantinescu CS, Gowland Pa. Increased iron accumulation occurs in the earliest stages of demyelinating disease: an ultra-high field susceptibility mapping study in Clinically Isolated Syndrome. Mult Scler. Jun; 2013 19(7):896–903. http://-www.ncbi.nlm.nih.gov/pubmed/23139386. [PubMed: 23139386]

Alexander GE, DeLong MR, Strick PL. Parallel Organization of Functionally Segregated Circuits Linking Basal Ganglia and Cortex. Annual Review of Neuroscience. 1986; 9(1):357–381. http://neuro.annualreviews.org/cgi/doi/10.1146/-annurev.neuro.9.1.357.

Audoin B, Zaaraoui W, Reuter F, Rico A, Malikova I, Confort-Gouny S, Cozzone PJ, Pelletier J, Ranjeva JP. Atrophy mainly affects the limbic system and the deep grey matter at the first stage of multiple sclerosis. Journal of Neurology, Neurosurgery and Psychiatry. 2009; 81:690–695. http://jnnp.bmj.com/content/81/6/-690.full.html#ref-list-1.

Axer H, Niemann K. Terminology of the thalamus and its representation in a part-whole relation. Meth Inform Med. 1994; 33:488–495. http://www.schattauer.de/en/-magazine/subject-areas/journals-a-z/methods/contents/archive/issue/special/-manuscript/14234/download.html. [PubMed: 7869946]

Bagnato F, Hametner S, Yao B, van Gelderen P, Merkle H, Cantor FK, Lassmann H, Duyn JH. Tracking iron in multiple sclerosis: a combined imaging and histopathological study at 7 Tesla. Brain. Dec; 2011 134(12):3599–3612. http://-www.brain.oxfordjournals.org/cgi/doi/10.1093/brain/awr278.

Banati RB. Visualising microglial activation in vivo. Glia. 2002; 40(2):206–217. [PubMed: 12379908]

Banati RB, Cagnin a, Brooks DJ, Gunn RN, Myers R, Jones T, Birch R, Anand P. Long-term trans-synaptic glial responses in the human thalamus after peripheral nerve injury. Neuroreport. 2001; 12(16):3439–3442. [PubMed: 11733686]

Banati RB, Newcombe J, Gunn RN, Cagnin a, Turkheimer F, Heppner F, Price G, Wegner F, Giovannoni G, Miller DH, Perkin GD, Smith T, Hewson aK, Bydder G, Kreutzberg GW, Jones T, Cuzner ML, Myers R. The peripheral benzodiazepine binding site in the brain in multiple sclerosis: quantitative in vivo imaging of microglia as a measure of disease activity. Brain. 2000; 123(Pt 1):2321–2337. [PubMed: 11050032]

Bartzokis G, Tishler TA, Lu PH, Villablanca JP, Altshuler LL, Carter M, Huang D, Edwards N, Mintz J. Brain ferritin iron may influence age- and gender-related risks of neurodegeneration. Neurobiol Aging. Mar; 2007 28(3):414–23. http://-www.ncbi.nlm.nih.gov/pubmed/16563566. [PubMed: 16563566]

Batista S, Zivadinov R, Hoogs M, Bergsland NP, Heininen-Brown M, Dwyer MG, Weinstock-Guttman B, Benedict RHB. Basal ganglia, thalamus and neocortical atrophy predicting slowed cognitive

processing in multiple sclerosis. Journal of Neurology. 2012; 259(1):139–146. [PubMed: 21720932]

Behrens TEJ, Johansen-Berg H, Woolrich MW, Smith SM, Wheeler-Kingshott CaM, Boulby Pa, Barker GJ, Sillery EL, Sheehan K, Ciccarelli O, Thompson aJ, Brady JM, Matthews PM. Non-invasive mapping of connections between human thalamus and cortex using diffusion imaging. Nature neuroscience. 2003; 6(7):750–7. http://www.ncbi.nlm.nih.gov/pubmed/12808459. [PubMed: 12808459]

Benarroch EE. Pulvinar: Associative role in cortical function and clinical correlations. Neurology. 2015; 84(7):738–747. [PubMed: 25609762]

Bergsland N, Agostini S, Laganà MM, Mancuso R, Mendozzi L, Tavazzi E, Cecconi P, Clerici M, Baglio F. Serum iron concentration is associated with subcortical deep gray matter iron levels in multiple sclerosis patients. NeuroReport. 2017; 28(11):645–648. http://insights.ovid.com/crossref?an=00001756-201708020-00008. [PubMed: 28509815]

Bergsland NP, Horakova D, Dwyer MG, Dolezal O, Seidl ZK, Vaneckova M, Krasensky J, Havrdova E, Zivadinov R. Subcortical and cortical gray matter atrophy in a large sample of patients with clinically isolated syndrome and early relapsing-remitting multiple sclerosis. American Journal of Neuroradiology. 2012; 33(8):1573–1578. [PubMed: 22499842]

Bergsland NP, Zivadinov R, Dwyer MG, Weinstock-Guttman B, Benedict RH. Localized atrophy of the thalamus and slowed cognitive processing speed in MS patients. Mult Scler. Sep; 2016 22(10): 1327–36. http://www.ncbi.nlm.nih.gov/pubmed/-26541795. [PubMed: 26541795]

Bermel, Ra, Puli, SR., Rudick, Ra, Weinstock-Guttman, B., Fisher, E., Munschauer, FE., Bakshi, R. Prediction of longitudinal brain atrophy in multiple sclerosis by gray matter magnetic resonance imaging T2 hypointensity. Archives of neurology. 2005; 62(9):1371–6. http://www.ncbi.nlm.nih.gov/pubmed/16157744. [PubMed: 16157744]

Bian W, Tranvinh E, Tourdias T, Han M, Liu T, Wang Y, Rutt B, Zeineh MM. In Vivo 7T MR Quantitative Susceptibility Mapping Reveals Opposite Susceptibility Contrast between Cortical and White Matter Lesions in Multiple Sclerosis. American Journal of Neuroradiology. Oct; 2016 37(10):1808–1815. http://-www.ajnr.org/cgi/doi/10.3174/ajnr.A4830.

Bilgic B, Pfefferbaum A, Rohlfing T, Sullivan EV, Adalsteinsson E. MRI estimates of brain iron concentration in normal aging using quantitative susceptibility mapping. NeuroImage. Feb; 2012 59(3):2625–2635. http://www.ncbi.nlm.nih.gov/pubmed/-21925274http://www.pubmedcentral.nih.gov/-articlerender.fcgi?artid=3254708&tool=pmcentrez&rendertype=abstracthttp://-linkinghub.elsevier.com/retrieve/pii/S1053811911010093. [PubMed: 21925274]

Bisecco A, Rocca MA, Pagani E, Mancini L, Enzinger C, Gallo A, Vrenken H, Stromillo ML, Copetti M, Thomas DL, Fazekas F, Tedeschi G, Barkhof F, Stefano ND, Filippi M. Connectivity-based parcellation of the thalamus in multiple sclerosis and its implications for cognitive impairment: A multicenter study. Human Brain Mapping. 2015; 36(7):2809–2825. [PubMed: 25873194]

Bisecco, A., Stamenova, S., Caiazzo, G., D'Ambrosio, A., Sacco, R., Docimo, R., Esposito, S., Cirillo, M., Esposito, F., Bonavita, S., Tedeschi, G., Gallo, A. Attention and processing speed performance in multiple sclerosis is mostly related to thalamic volume. Brain Imaging and Behavior. Jan. 2017 http://dx.doi.org/10.1007/s11682-016-9667-6http://link.springer.com/10.1007/s11682-016-9667-6

Blazejewska AI, Al-Radaideh AM, Wharton S, Lim SY, Bowtell RW, Constantinescu CS, Gowland Pa. Increase in the iron content of the substantia nigra and red nucleus in multiple sclerosis and clinically isolated syndrome: A 7 Tesla MRI study. Journal of Magnetic Resonance Imaging. Apr; 2015 41(4):1065–1070. http://www.ncbi.nlm.nih.gov/pubmed/24841344http://doi.wiley.com/10.1002/-jmri.24644. [PubMed: 24841344]

Blinkenberg, M., Rune, K., Jensen, CV., Ravnborg, M., Kyllingsbæk, S., Holm, S., Paulson, OB., Sørensen, PS. Cortical cerebral metabolism correlates with MRI lesion load and cognitive dysfunction in MS. 2000. http://www.ncbi.nlm.nih.gov/pubmed/-10680783

Burgetova, A., Dusek, P., Vaneckova, M., Horakova, D., Langkammer, C., Krasensky, J., Sobisek, L., Matras, P., Masek, M., Seidl, Z. Thalamic Iron Differentiates Primary-Progressive and Relapsing-Remitting Multiple Sclerosis. American Journal of Neuroradiology. 2017. http://www.ajnr.org/lookup/doi/10.3174/ajnr.A5166

Calabrese M, Atzori M, Bernardi V, Morra A, Romualdi C, Rinaldi L, McAuliffe MJM, Barachino L, Perini P, Fischl B, Battistin L, Gallo P. Cortical atrophy is relevant in multiple sclerosis at clinical onset. J Neurol. 2007; 254(9):1212–1220. [PubMed: 17361339]

Calabrese M, Rinaldi F, Mattisi I, Bernardi V, Favaretto A, Perini P, Gallo P. The predictive value of gray matter atrophy in clinically isolated syndromes. Neurology. Jul; 2011 77(3):257–263. http://www.neurology.org/cgi/doi/10.1212/-WNL.0b013e318220abd4. [PubMed: 21613600]

Charil A, Yousry TA, Rovaris M, Barkhof F, De Stefano N, Fazekas F, Miller DH, Montalban X, Simon JH, Polman CH, Filippi M. MRI and the diagnosis of multiple sclerosis: expanding the concept of “no better explanation”. Lancet Neurol. Oct; 2006 5(10):841–52. http://www.ncbi.nlm.nih.gov/pubmed/16987731. [PubMed: 16987731]

Chen W, Gauthier Sa, Gupta A, Comunale J, Liu T, Wang S, Pei M, Pitt D, Wang Y. Quantitative Susceptibility Mapping of Multiple Sclerosis Lesions at Various Ages. Radiology. Apr; 2014 271(1):183–192. http://www.ncbi.nlm.nih.gov/pubmed/-24475808http://pubs.rsna.org/doi/10.1148/radiol.13130353. [PubMed: 24475808]

Chen W, Zhu W, Kovanlikaya I, Kovanlikaya A, Liu T, Wang S, Salustri C, Wang Y. Intracranial calcifications and hemorrhages: characterization with quantitative susceptibility mapping. Radiology. Feb; 2014 270(2):496–505. http://pubs.rsna.org/-doi/abs/10.1148/radiology.13122640http://www.ncbi.nlm.nih.gov/pubmed/24126366. [PubMed: 24126366]

Cheng G, Kong RH, Zhang LM, Zhang JN. Mitochondria in traumatic brain injury and mitochondrial-targeted multipotential therapeutic strategies. British Journal of Pharmacology. 2012; 167(4):699–719. [PubMed: 23003569]

Cherubini A, Péran P, Caltagirone C, Sabatini U, Spalletta G. Aging of subcortical nuclei: microstructural, mineralization and atrophy modifications measured in vivo using MRI. NeuroImage. Oct; 2009 48(1):29–36. http://dx.doi.org/10.1016/-j.neuroimage.2009.06.035. [PubMed: 19540925]

Cifelli A, Arridge M, Jezzard P, Esiri MM, Palace J, Matthews PM. Thalamic neurodegeneration in multiple sclerosis. Annals of Neurology. 2002; 52(5):650–653. [PubMed: 12402265]

Cobzas D, Sun H, Walsh AJ, Lebel RM, Blevins G, Wilman AH. Subcortical gray matter segmentation and voxel-based analysis using transverse relaxation and quantitative susceptibility mapping with application to multiple sclerosis. J Magn Reson Imaging. Dec; 2015 42(6):1601–1610. http://doi.wiley.com/10.1002/-jmri.24951. [PubMed: 25980643]

Connor JR, Menzies SL. Relationship of iron to oligondendrocytes and myelination. Glia. Jun; 1996 17(2):83–93. http://doi.wiley.com/10.1002/(SICI)1098-1136(199606)17:2%3C83::AID-GLIA1%3E3.0.CO;2-7. [PubMed: 8776576]

Contreras L, Drago I, Zampese E, Pozzan T. Mitochondria: The calcium connection. Biochimica et Biophysica Acta - Bioenergetics. 2010; 1797(6–7):607–618. http://dx.doi.org/10.1016/j.bbabio.2010.05.005.

Cronin MJ, Wharton SJ, Al-Radaideh AM, Constantinescu C, Evangelou N, Bowtell R, Gowland PA. A comparison of phase imaging and quantitative susceptibility mapping in the imaging of multiple sclerosis lesions at ultrahigh field. Magnetic Resonance Materials in Physics, Biology and Medicine. 2016:1–15.

Deh K, Nguyen TD, Eskreis-Winkler S, Prince MR, Spincemaille P, Gauthier S, Kovanlikaya I, Zhang Y, Wang Y. Reproducibility of quantitative susceptibility mapping in the brain at two field strengths from two vendors. J Magn Reson Imaging. Dec; 2015 42(6):1592–1600. http://doi.wiley.com/10.1002/jmri.24943. [PubMed: 25960320]

Deistung A, Schäfer A, Schweser F, Biedermann U, Turner R, Reichenbach JR. Toward in vivo histology: a comparison of quantitative susceptibility mapping (QSM) with magnitude-, phase-, and R2*-imaging at ultra-high magnetic field strength. NeuroImage. Jan.2013 65:299–314. http://www.ncbi.nlm.nih.gov/pubmed/23036448. [PubMed: 23036448]

Dietrich O, Levin J, Ahmadi SA, Plate A, Reiser MF, Bötzel K, Giese A, Ertl-Wagner B. MR imaging differentiation of Fe2+ and Fe3+ based on relaxation and magnetic susceptibility properties. Neuroradiology. Apr; 2017 59(4):403–409. http://link.springer.com/10.1007/s00234-017-1813-3. [PubMed: 28324122]

Doring TM, Granado V, Rueda F, Deistung A, Reichenbach JR, Tukamoto G, Gasparetto EL, Schweser F. Quantitative Susceptibility Mapping Indicates a Disturbed Brain Iron Homeostasis in

Neuromyelitis Optica â€“ A Pilot Study. PLoS ONE. 2016; 11(5):e0155027. http://dx.plos.org/10.1371/journal.pone.0155027. [PubMed: 27171423]

Drayer BP, Burger P, Hurwitz B, Dawson D, Cain J. Reduced signal intensity on MR images of thalamus and putamen in multiple sclerosis: increased iron content? AJR. American journal of roentgenology. 1987; 149(2):357–63. http://-www.ncbi.nlm.nih.gov/pubmed/3496764. [PubMed: 3496764]

Du S, Sah SK, Zeng C, Wang J, Liu Y, Xiong H, Li Y. Iron deposition in the gray matter in patients with relapse-remitting multiple sclerosis: A longitudinal study using three-dimensional (3D)-enhanced T2???-weighted angiography (ESWAN). European Journal of Radiology. 2015; 84(7): 1325–1332. http://dx.doi.org/10.1016/-j.ejrad.2015.04.013. [PubMed: 25959392]

Duyn JH. MR susceptibility imaging. J Magn Reson. Apr.2013 229:198–207. http://-www.ncbi.nlm.nih.gov/pubmed/23273840. [PubMed: 23273840]

Elkady AM, Cobzas D, Sun H, Blevins G, Wilman AH. Progressive iron accumulation across multiple sclerosis phenotypes revealed by sparse classification of deep gray matter. J Magn Reson Imaging. 2017 (epub).

Elkady AM, Sun H, Wilman AH. Importance of extended spatial coverage for quantitative susceptibility mapping of iron-rich deep grey matter. Magnetic resonance imaging. 2015; 34(4): 574–578. http://linkinghub.elsevier.com/retrieve/pii/-S0730725X15003367%5Cnhttp://www.ncbi.nlm.nih.gov/pubmed/26721523. [PubMed: 26721523]

Eskreis-Winkler S, Deh K, Gupta A, Liu T, Wisnieff C, Jin M, Gauthier Sa, Wang Y, Spincemaille P. Multiple sclerosis lesion geometry in quantitative susceptibility mapping (QSM) and phase imaging. J Magn Reson Imaging. Aug.2014 00:1–6. http://www.ncbi.nlm.nih.gov/pubmed/25174493.

Fama R, Sullivan EV. Thalamic structures and associated cognitive functions: Relations with age and aging. Neuroscience and Biobehavioral Reviews. 2014; 54:29–37. http://dx.doi.org/10.1016/j.neubiorev.2015.03.008.

Federal Committee on Anatomical Terminology. Terminologia Anatomica. 1st. Thieme; Stuttgart, Germany: 1998.

Feng, X., Deistung, A., Reichenbach, JR. Quantitative susceptibility mapping (QSM) and R2* in the human brain at 3 T. Z Med Phys. Jun. 2017 http://-linkinghub.elsevier.com/retrieve/pii/S0939388916301143

Francois C, Nguyen-Legros J, Percheron G. Topographical and cytological localization of iron in rat and monkey brains. Brain Res. Jun; 1981 215(1–2):317–322. http://-linkinghub.elsevier.com/retrieve/pii/0006899381905102. [PubMed: 7260591]

Frischer JM, Bramow S, Dal-Bianco A, Lucchinetti CF, Rauschka H, Schmidbauer M, Laursen H, Sorensen PS, Lassmann H. The relation between inflammation and neurodegeneration in multiple sclerosis brains. Brain. May; 2009 132(5):1175–1189. https://academic.oup.com/brain/article-lookup/doi/10.1093/brain/awp070. [PubMed: 19339255]

Fujiwara, E., Kmech, J., Cobzas, D., Sun, H., Seres, P., Blevins, G., Wilman, AH. Cognitive Implications of Deep Gray Matter Iron in Multiple Sclerosis; American Journal of Neuroradiology. Feb. 2017 p. 7-11.http://www.ajnr.org/lookup/doi/10.3174/ajnr.A5109

Gabilondo I, Martínez-Lapiscina EH, Martínez-Heras E, Fraga-Pumar E, Llufriu S, Ortiz S, Bullich S, Sepulveda M, Falcon C, Berenguer J, Saiz A, Sanchez-Dalmau B, Villoslada P. Trans-synaptic axonal degeneration in the visual pathway in multiple sclerosis. Annals of Neurology. 2014; 75(1): 98–107. [PubMed: 24114885]

Ge Y, Jensen JH, Lu H, Helpern Ja, Miles L, Inglese M, Babb JS, Herbert J, Grossman RI. Quantitative assessment of iron accumulation in the deep gray matter of multiple sclerosis by magnetic field correlation imaging. Am J Roentgenol. Oct; 2007 28(9):1639–44. http://www.ncbi.nlm.nih.gov/pubmed/17893225.

Groeschel S, Hagberg GE, Schultz T, Balla DZ, Klose U, Hauser TK, Nägele T, Bieri O, Prasloski T, MacKay AL, Krägeloh-Mann I, Scheffler K. Assessing White Matter Microstructure in Brain Regions with Different Myelin Architecture Using MRI. Plos One. 2016; 11(11):e0167274. http://dx.plos.org/10.1371/-journal.pone.0167274. [PubMed: 27898701]

Guadalupe, T., Mathias, SR., VanErp, TGM., Whelan, CD., Zwiers, MP., Abe, Y., Abramovic, L., Agartz, I., Andreassen, OA., Arias-Vásquez, A., Aribisala, BS., Armstrong, NJ., Arolt, V., Artiges, E., Ayesa-Arriola, R., Baboyan, VG., Banaschewski, T., Barker, G., Bastin, ME., Baune, BT., Blangero, J., Bokde, AL., Boedhoe, PS., Bose, A., Brem, S., Brodaty, H., Bromberg, U., Brooks, S., Büchel, C., Buitelaar, J., Calhoun, VD., Cannon, DM., Cattrell, A., Cheng, Y., Conrod, PJ., Conzelmann, A., Corvin, A., Crespo-Facorro, B., Crivello, F., Dannlowski, U., de Zubicaray, GI., de Zwarte, SM., Deary, IJ., Desrivières, S., Doan, NT., Donohoe, G., Dørum, ES., Ehrlich, S., Espeseth, T., Fernández, G., Flor, H., Fouche, JP., Frouin, V., Fukunaga, M., Gallinat, J., Garavan, H., Gill, M., Suarez, AG., Gowland, P., Grabe, HJ., Grotegerd, D., Gruber, O., Hagenaars, S., Hashimoto, R., Hauser, TU., Heinz, A., Hibar, DP., Hoekstra, PJ., Hoogman, M., Howells, FM., Hu, H., Hulshoff Pol, HE., Huyser, C., Ittermann, B., Jahanshad, N., Jönsson, EG., Jurk, S., Kahn, RS., Kelly, S., Kraemer, B., Kugel, H., Kwon, JS., Lemaitre, H., Lesch, KP., Lochner, C., Luciano, M., Marquand, AF., Martin, NG., Martínez-Zalacaín, I., Martinot, JL., Mataix-Cols, D., Mather, K., McDonald, C., McMahon, KL., Medland, SE., Menchón, JM., Morris, DW., Mothersill, O., Maniega, SM., Mwangi, B., Nakamae, T., Nakao, T., Narayanaswaamy, JC., Nees, F., Nordvik, JE., Onnink, AMH., Opel, N., Ophoff, R., Paillère Martinot, ML., Papadopoulos Orfanos, D., Pauli, P., Paus, T., Poustka, L., Reddy, JY., Renteria, ME., Roiz-Santiáñez, R., Roos, A., Royle, NA., Sachdev, P., Sánchez-Juan, P., Schmaal, L., Schumann, G., Shumskaya, E., Smolka, MN., Soares, JC., Soriano-Mas, C., Stein, DJ., Strike, LT., Toro, R., Turner, JA., Tzourio-Mazoyer, N., Uhlmann, A., Hernández, MV., van den Heuvel, OA., van der Meer, D., van Haren, NEM., Veltman, DJ., Venkatasubramanian, G., Vetter, NC., Vuletic, D., Walitza, S., Walter, H., Walton, E., Wang, Z., Wardlaw, J., Wen, W., Westlye, LT., Whelan, R., Wittfeld, K., Wolfers, T., Wright, MJ., Xu, J., Xu, X., Yun, JY., Zhao, J., Franke, B., Thompson, PM., Glahn, DC., Mazoyer, B., Fisher, SE., Francks, C. Human subcortical brain asymmetries in 15,847 people worldwide reveal effects of age and sex. Brain Imaging and Behavior. Oct. 2016 http://link.springer.com/10.1007/s11682-016-9629-z

Haacke EM, Garbern J, Miao Y, Habib CA, Liu M. Iron stores and cerebral veins in MS studied by susceptibility weighted imaging. Int Angiol. 2010; 29(2):149–57. http://www.ncbi.nlm.nih.gov/pubmed/20351671. [PubMed: 20351671]

Haacke EM, Liu S, Buch S, Zheng W, Wu D, Ye Y. Quantitative susceptibility mapping: current status and future directions. Magn Reson Imaging. Jan; 2015 33(1):1–25. http://www.ncbi.nlm.nih.gov/pubmed/25267705http://-linkinghub.elsevier.com/retrieve/pii/S0730725X14002926. [PubMed: 25267705]

Habib CA, Liu M, Bawany N, Garbern J, Krumbein I, Mentzel HJ, Reichenbach JR, Magnano CR, Zivadinov R, Haacke EM. Assessing abnormal iron content in the deep gray matter of patients with multiple sclerosis versus healthy controls. Am J Roentgenol. Feb; 2012 33(2):252–8. http://www.ajnr.org/content/33/2/252.shorthttp://www.ncbi.nlm.nih.gov/pubmed/22116106.

Hagemeier J, Dwyer MG, Bergsland NP, Schweser F, Magnano CR, Heininen-Brown M, Ramasamy DP, Carl E, Kennedy C, Melia R, Polak P, Deistung A, Geurts JJG, Reichenbach JR, Zivadinov R. Effect of age on MRI phase behavior in the subcortical deep gray matter of healthy individuals. Am J Neuroradiol. May; 2013 34(11):2144–51. http://www.ncbi.nlm.nih.gov/pubmed/23721902. [PubMed: 23721902]

Hagemeier J, Weinstock-Guttman B, Bergsland NP, Heininen-Brown M, Carl E, Kennedy C, Magnano CR, Hojnacki D, Dwyer MG, Zivadinov R. Iron deposition on SWI-filtered phase in the subcortical deep gray matter of patients with clinically isolated syndrome may precede structure-specific atrophy. Am J Neuroradiol. Sep; 2012 33(8):1596–601. http://www.ncbi.nlm.nih.gov/pubmed/22460343. [PubMed: 22460343]

Hagemeier J, Yeh EA, Brown MH, Bergsland NP, Dwyer MG, Carl E, Weinstock-Guttman B, Zivadinov R. Iron content of the pulvinar nucleus of the thalamus is increased in adolescent multiple sclerosis. Multiple Sclerosis Journal. Apr; 2013 19(5):567–576. http://www.ncbi.nlm.nih.gov/pubmed/22968543http://-msj.sagepub.com/cgi/doi/10.1177/1352458512459289. [PubMed: 22968543]

Hagemeier, J., Zivadinov, R., Dwyer, MG., Polak, P., Bergsland, NP., Weinstock-Guttman, B., Zalis, J., Deistung, A., Reichenbach, JR., Schweser, F. Changes of deep gray matter magnetic susceptibility over 2 years in multiple sclerosis and healthy control brain. NeuroImage: Clinical. Apr. 2017 (epub) http://linkinghub.elsevier.com/retrieve/-pii/S2213158217300840

Haider L, Simeonidou C, Steinberger G, Hametner S, Grigoriadis N, Deretzi G, Kovacs GG, Kutzelnigg A, Lassmann H, Frischer JM. Multiple sclerosis deep grey matter: the relation between demyelination, neurodegeneration, inflammation and iron. J Neurol Neurosurg Psychiatry. Dec; 2014 85(12):1386–1395. http://-www.ncbi.nlm.nih.gov/pubmed/24899728http://jnnp.bmj.com/lookup/doi/10.1136/-jnnp-2014-307712. [PubMed: 24899728]

Hallgren B, Sourander P. The effect of age on the non-haemin iron in the human brain. J Neurochem. 1958; 3:41–51. [PubMed: 13611557]

Hametner S, Wimmer I, Haider L, Pfeifenbring S, Brück W, Lassmann H. Iron and neurodegeneration in the multiple sclerosis brain. Ann Neurol. Dec; 2013 74(6):848–861. http://www.ncbi.nlm.nih.gov/pubmed/23868451http://doi.wiley.com/10.1002/-ana.23974. [PubMed: 23868451]

Hammond KE, Lupo JM, Xu D, Metcalf M, Kelley DAC, Pelletier D, Chang SM, Mukherjee P, Vigneron DB, Nelson SJ. Development of a robust method for generating 7.0 T multichannel phase images of the brain with application to normal volunteers and patients with neurological diseases. NeuroImage. Feb; 2008 39(4):1682–1692. http://dx.doi.org/10.1016/j.neuroimage.2007.10.037. [PubMed: 18096412]

Hanspach, J., Dwyer, MG., Bergsland, NP., Feng, X., Hagemeier, J., Bertolino, N., Polak, P., Reichenbach, JR., Zivadinov, R., Schweser, F. Methods for the computation of templates from quantitative magnetic susceptibility maps (QSM): Toward improved atlas- and voxel-based analyses (VBA). Journal of Magnetic Resonance Imaging. Mar. 2017 http://doi.wiley.com/10.1002/jmri.25671

Harrison DM, Li X, Liu H, Jones CK, Caffo B, Calabresi PA, van Zijl PCM. Lesion Heterogeneity on High-Field Susceptibility MRI Is Associated with Multiple Sclerosis Severity. Am J Neuroradiol. Aug; 2016 37(8):1447–1453. http://-www.ajnr.org/cgi/doi/10.3174/ajnr.A4726. [PubMed: 26939635]

Henry RG, Shieh M, Amirbekian B, Chung S, Okuda DT, Pelletier D. Connecting white matter injury and thalamic atrophy in clinically isolated syndromes. Journal of the Neurological Sciences. 2009; 282(1–2):61–66. http://dx.doi.org/10.1016/-j.jns.2009.02.379. [PubMed: 19394969]

Henry RG, Shieh M, Okuda DT, Evangelista A, Gorno-Tempini ML, Pelletier D. Regional grey matter atrophy in clinically isolated syndromes at presentation. J Neurol Neurosurg Psychiatry. 2008; 79:1236–1244. February 2016. http://jnnp.bmj.com/-content/79/11/1236.full.html%5Cnhttp://jnnp.bmj.com/content/79/11/-1236.full.html#related-urls%5Cnhttp://jnnp.bmj.com/content/79/11/-1236.full.html%23ref-list-1. [PubMed: 18469033]

Hernández-Torres E, Wiggermann V, Li DK, Machan L, Sadovnick AD, Hametner S, Rauscher A. Iron loss occurs in the deep gray matter of multiple sclerosis patients. Proc Intl Soc Mag Reson Med. 2017; 2017; 25:790.

Herranz E, Giannì C, Louapre C, Treaba CA, Govindarajan ST, Ouellette R, Loggia ML, Sloane JA, Madigan N, Izquierdo-Garcia D, Ward N, Mangeat G, Granberg T, Klawiter EC, Catana C, Hooker JM, Taylor N, Ionete C, Kinkel RP, Mainero C. Neuroinflammatory component of gray matter pathology in multiple sclerosis. Ann Neurol. Nov; 2016 80(5):776–790. http://doi.wiley.com/-10.1002/ana.24791. [PubMed: 27686563]

Hill JM, Switzer RC III. The regional distribution and cellular localization of iron in the rat brain. Neuroscience. Mar; 1984 11(3):595–603. http://linkinghub.elsevier.com/-retrieve/pii/0306452284900460. [PubMed: 6717804]

Houtchens MK, Benedict RHB, Killiany R, Sharma J, Jaisani Z, Singh B, Weinstock-Guttman B, Guttmann CRG, Bakshi R. Thalamic atrophy and cognition in multiple sclerosis. Neurology. 2007; 69(12):1213–1223. [PubMed: 17875909]

Howell OW, Reeves CA, Nicholas R, Carassiti D, Radotra B, Gentleman SM, Serafini B, Aloisi F, Roncaroli F, Magliozzi R, Reynolds R. Meningeal inflammation is widespread and linked to cortical pathology in multiple sclerosis. Brain. 2011; 134(9):2755–2771. [PubMed: 21840891]

Hughes EJ, Bond J, Svrckova P, Makropoulos A, Ball G, Sharp DJ, Edwards aD, Hajnal JV, Counsell SJ. Regional changes in thalamic shape and volume with increasing age. NeuroImage. Jul; 2012 63(3):1134–1142. http://dx.doi.org/-10.1016/j.neuroimage.2012.07.043http://www.ncbi.nlm.nih.gov/pubmed/22846656. [PubMed: 22846656]

Johansen-Berg H, Behrens TEJ, Sillery E, Ciccarelli O, Thompson AJ, Smith SM, Matthews PM. Functional-anatomical validation and individual variation of diffusion tractography-based segmentation of the human thalamus. Cerebral cortex (New York, NY: 1991). Jan; 2005 15(1):31–9. http://-www.cercor.oupjournals.org/cgi/doi/10.1093/cercor/bhh105http://-www.ncbi.nlm.nih.gov/pubmed/15238447.

Jones, EG. Holstege, G., editor. The anatomy of sensory relay functions in the thalamus; Progress in Brain Research. 87th1991. p. 29-52.Ch 3http://-linkinghub.elsevier.com/retrieve/pii/S0079612308630460

Kakeda S, Futatsuya K, Ide S, Watanabe K, Miyata M, Moriya J, Ogasawara A, Sato T, Narimatsu H, Okada K, Uozumi T, Liu T, Wang Y, Korogi Y. Improved Detection of Cortical Gray Matter Involvement in Multiple Sclerosis with Quantitative Susceptibility Mapping. Acad Radiol. Nov; 2015 22(11):1427–1432. http://-linkinghub.elsevier.com/retrieve/pii/S1076633215003281. [PubMed: 26342769]

Kanaan, AS., Anwander, A., Schäfer, A., Bilgic, B., Schlumm, T., Near, J., Müller-Vahl, K., Möller, HE. Proc Intl Soc Mag Reson Med. Vol. 25. Honolulu, HI; 2017. 2017. QSM meets MRS: The influence of subcortical iron on glutamatergic neurotransmission in a movement disorder population; p. 4649

Kanowski, M., Voges, J., Buentjen, L., Stadler, J., Heinze, HJ., Tempelmann, C. Direct Visualization of Anatomic Subfields within the Superior Aspect of the Human Lateral Thalamus by MRI at 7T. AJNR; American journal of neuroradiology. 2014. p. 1-7.http://www.ncbi.nlm.nih.gov/pubmed/24852290

Kauzner U, Kang Y, Morris E, Nealon N, Perumal JS, Vartanian T, Gauthier SA. Uptake of [C11]PJK11195 in the thalamus of Multiple Sclerosis (MS) patients versus Healthy Controls (HC). ECTRIMS. 20162016

Khalil M, Enzinger C, Langkammer C, Tscherner M, Wallner-Blazek M, Jehna M, Ropele S, Fuchs S, Fazekas F. Quantitative assessment of brain iron by R2* relaxometry in patients with clinically isolated syndrome and relapsing-remitting multiple sclerosis. Mult Scler. Sep; 2009 15(9):1048–54. http://www.ncbi.nlm.nih.gov/pubmed/-19556316. [PubMed: 19556316]

Khalil M, Langkammer C, Pichler A, Pinter D, Gattringer T, Bachmaier G, Ropele S, Fuchs S, Enzinger C, Fazekas F. Dynamics of brain iron levels in multiple sclerosis: A longitudinal 3T MRI study. Neurology. 2015; 84(24):2396–2402. [PubMed: 25979698]

Kuchcinski G, Munsch F, Lopes R, Bigourdan A, Su J, Sagnier S, Renou P, Pruvo JP, Rutt BK, Dousset V, Sibon I, Tourdias T. Thalamic alterations remote to infarct appear as focal iron accumulation and impact clinical outcome. Brain. Jul; 2017 140(7):1932–1946. https://academic.oup.com/brain/article-lookup/doi/10.1093/-brain/awx114. [PubMed: 28549087]

Kurtzke JF. Rating neurologic impairment in multiple sclerosis: an expanded disability status scale (EDSS). Neurology. 1983; 33(11):1444–1452. [PubMed: 6685237]

Kutzelnigg A, Lassmann H. Cortical lesions and brain atrophy in MS. Journal of the Neurological Sciences. 2005; 233(1–2):55–59. [PubMed: 15893328]

Kutzelnigg A, Lucchinetti CF, Stadelmann C, Br??ck W, Rauschka H, Bergmann M, Schmidbauer M, Parisi JE, Lassmann H. Cortical demyelination and diffuse white matter injury in multiple sclerosis. Brain. 2005; 128(11):2705–2712. [PubMed: 16230320]

Langkammer C, Bredies K, Poser BA, Barth M, Reishofer G, Fan AP, Bilgic B, Fazekas F, Mainero C, Ropele S. Fast quantitative susceptibility mapping using 3D EPI and total generalized variation. NeuroImage. 2015; 111:622–630. February 2016. [PubMed: 25731991]

Langkammer C, Liu T, Khalil M, Enzinger C, Jehna M, Fuchs S, Fazekas F, Wang Y, Ropele S. Quantitative susceptibility mapping in multiple sclerosis. Radiology. May; 2013 267(2):551–9. http://www.ncbi.nlm.nih.gov/pubmed/23315661. [PubMed: 23315661]

Langkammer C, Schweser F, Krebs N, Deistung A, Goessler W, Scheurer E, Sommer K, Reishofer G, Yen K, Fazekas F, Ropele S, Reichenbach JR. Quantitative susceptibility mapping (QSM) as a means to measure brain iron? A post mortem validation study. NeuroImage. May; 2012 62(3):1593–1599. http://-www.ncbi.nlm.nih.gov/pubmed/22634862. [PubMed: 22634862]

Lansley J, Mataix-Cols D, Grau M, Radua J, Sastre-Garriga J. Localized grey matter atrophy in multiple sclerosis: A meta-analysis of voxel-based morphometry studies and associations with

functional disability. Neuroscience and Biobehavioral Reviews. 2013; 37(5):819–830. http://dx.doi.org/10.1016/j.neubiorev.2013.03.006. [PubMed: 23518268]

Lassmann H, van Horssen J, Mahad D. Progressive multiple sclerosis: pathology and pathogenesis. Nature Reviews Neurology. Sep; 2012 8(11):647–656. http://-www.nature.com/doifinder/10.1038/nrneurol.2012.168. [PubMed: 23007702]

Lebel RM, Eissa A, Seres P, Blevins G, Wilman AH. Quantitative high-field imaging of sub-cortical gray matter in multiple sclerosis. Mult Scler. Apr; 2012 18(4):433–41. http://www.ncbi.nlm.nih.gov/pubmed/22032862. [PubMed: 22032862]

Lewin A, Hamilton S, Witkover A, Langford P, Nicholas R, Chataway J, Bangham CR. Free serum haemoglobin is associated with brain atrophy in secondary progressive multiple sclerosis. Wellcome Open Research. Nov.2016 1(0):10. https://-wellcomeopenresearch.org/articles/1-10/v1. [PubMed: 27996064]

Li W, Wu B, Liu C. Quantitative susceptibility mapping of human brain reflects spatial variation in tissue composition. NeuroImage. Apr; 2011 55(4):1645–56. http://-www.pubmedcentral.nih.gov/-articlerender.fcgi?artid=3062654&tool=pmcentrez&rendertype=abstract. [PubMed: 21224002]

Li X, Harrison DM, Liu H, Jones CK, Oh J, Calabresi PA, van Zijl PCM. Magnetic susceptibility contrast variations in multiple sclerosis lesions. J Magn Reson Imaging. Feb; 2016 43(2):463–473. http://doi.wiley.com/10.1002/jmri.24976. [PubMed: 26073973]

Lin PY, Chao TC, Wu ML. Quantitative Susceptibility Mapping of Human Brain at 3T: A Multisite Reproducibility Study. Am J Neurology. Mar; 2015 36(3):467–474. http://www.ncbi.nlm.nih.gov/pubmed/25339652http://www.ajnr.org/cgi/doi/10.3174/-ajnr.A4137.

Liu C, Li W, Tong KA, Yeom KW, Kuzminski S. Susceptibility-weighted imaging and quantitative susceptibility mapping in the brain. J Magn Reson Imaging. 2015; 42(1):23–41. [PubMed: 25270052]

Mathers LH. The synaptic organization of the cortical projection to the pulvinar of the squirrel monkey. The Journal of Comparative Neurology. Sep; 1972 146(1):43–59. http://-doi.wiley.com/10.1002/cne.901460104. [PubMed: 4627260]

Meguro R, Asano Y, Odagiri S, Li C, Shoumura K. Cellular and subcellular localizations of nonheme ferric and ferrous iron in the rat brain: a light and electron microscopic study by the perfusion-Perls and -Turnbull methods. Arch Histol Cytol. 2008; 71(4):205–222. http://joi.jlc.jst.go.jp/JST.JSTAGE/aohc/71.205?from=CrossRef. [PubMed: 19359804]

Metz A, Spatz H. Die Hortegaschen Zellen (= das sogenannte “dritte Element”) und über ihre funktionelle Bedeutung). Z ges Neuro Psychiat. 1924; 89(1):138–170.

Minagar A, Barnett MH, Benedict RHB, Pelletier D, Pirko I, Sahraian MA, Frohman E, Zivadinov R. The thalamus and multiple sclerosis: modern views on pathologic, imaging, and clinical aspects. Neurology. Jan; 2013 80(2):210–9. http://-www.ncbi.nlm.nih.gov/pubmed/23296131. [PubMed: 23296131]

Mitsumori F, Watanabe H, Takaya N. Estimation of brain iron concentration in vivo using a linear relationship between regional iron and apparent transverse relaxation rate of the tissue water at 4.7T. Magn Reson Med. Nov; 2009 62(5):1326–30. http://-www.ncbi.nlm.nih.gov/pubmed/19780172. [PubMed: 19780172]

Modica CM, Zivadinov R, Dwyer MG, Bergsland NP, Weeks aR, Benedict RHB. Iron and Volume in the Deep Gray Matter: Association with Cognitive Impairment in Multiple Sclerosis. Am J Neuroradiol. Jun.2014 i:1–6. http://-www.ncbi.nlm.nih.gov/pubmed/24948507.

Moore DF, Ye F, Schiffmann R, Butman Ja. Increased signal intensity in the pulvinar on T1-weighted images: a pathognomonic MR imaging sign of Fabry disease. Am J Roentgenol. 2003; 24(6):1096–101. http://www.ncbi.nlm.nih.gov/pubmed/12812932.

Morris CM, Candy JM, Oakley AE, Bloxham CA, Edwardson JA. Histochemical distribution of non-haem iron in the human brain. Acta Anat. Jan; 1992 144(3):235–57. http://www.ncbi.nlm.nih.gov/pubmed/1529678. [PubMed: 1529678]

Muhlau M, Buck D, Forschler A, Boucard CC, Arsic M, Schmidt P, Gaser C, Berthele A, Hoshi M, Jochim A, Kronsbein H, Zimmer C, Hemmer B, Ilg R. White-matter lesions drive deep gray-matter atrophy in early multiple sclerosis: support from structural MRI. Multiple Sclerosis

Journal. Oct; 2013 19(11):1485–1492. http://www.ncbi.nlm.nih.gov/pubmed/23462349http://msj.sagepub.com/cgi/doi/-10.1177/1352458513478673. [PubMed: 23462349]

Myers R, Manjil LG, Frackowiak RS, Cremer JE. [3H]PK 11195 and the localisation of secondary thalamic lesions following focal ischaemia in rat motor cortex. Neuroscience Letters. Nov; 1991 133(1):20–24. http://linkinghub.elsevier.com/retrieve/-pii/030439409190047W. [PubMed: 1791992]

Myers RH, Vonsattel JP, Paskevich PA, Kiely DK, Stevens TJ, Cupples L, Richardson EP, Bird ED. Decreased Neuronal and Increased Oligodendroglial Densities in Huntington's Disease Caudate Nucleus. J Neuropathol Exp Neurol. 1991; 50(6):729–742. [PubMed: 1836225]

Ogren MP, Hendrickson AE. The morphology and distribution of striate cortex terminals in the inferior and lateral subdivision of theMacaca monkey pulvinar. The Journal of Comparative Neurology. Nov; 1979 188(1):179–199. http://doi.wiley.com/-10.1002/cne.901880113. [PubMed: 115908]

Osteen CL, Giza CC, Hovda DA. Injury-induced alterations in N-methyl-D-aspartate receptor subunit composition contribute to prolonged 45calcium accumulation following lateral fluid percussion. Neuroscience. 2004; 128(2):305–322. [PubMed: 15350643]

Osteen CL, Moore AH, Prins ML, Hovda DA. Age-dependency of 45calcium accumulation following lateral fluid percussion: acute and delayed patterns. J Neurotrauma. 2001; 18(2):141–62. http://www.ncbi.nlm.nih.gov/pubmed/11229708. [PubMed: 11229708]

Özbay PS, Deistung A, Feng X, Nanz D, Reichenbach JR, Schweser F. A comprehensive numerical analysis of background phase correction with V-SHARP. NMR iBiomed. Apr.2017 30(4):e3550. http://doi.wiley.com/10.1002/nbm.3550.

Panov AV, Andreeva L, Greenamyre JT. Quantitative evaluation of the effects of mitochondrial permeability transition pore modifiers on accumulation of calcium phosphate: Comparison of rat liver and brain mitochondria. Archives of Biochemistry and Biophysics. 2004; 424(1):44–52. [PubMed: 15019835]

Pappata S, Levasseur M, Gunn RN, Myers R, Crouzel C, Syrota A, Jones T, Kreutzberg GW, Banati RB. Thalamic microglial activation in ischemic stroke detected in vivo by PET and [11C]PK11195. Neurology. Oct; 2000 55(7):1052–1054. http://www.neurology.org/cgi/doi/10.1212/WNL.55.7.1052. [PubMed: 11061271]

Persson N, Wu J, Zhang Q, Liu T, Shen J, Bao R, Ni M, Liu T, Wang Y, Spincemaille P. Age and sex related differences in subcortical brain iron concentrations among healthy adults. NeuroImage. 2015; 122:385–398. http://-linkinghub.elsevier.com/retrieve/pii/S1053811915006618. [PubMed: 26216277]

Philp DJ, Korgaonkar MS, Grieve SM. Thalamic volume and thalamo-cortical white matter tracts correlate with motor and verbal memory performance. NeuroImage. 2014; 91:77–83. http://dx.doi.org/10.1016/j.neuroimage.2013.12.057. [PubMed: 24401559]

Pitt D, Boster A, Pei W, Wohleb E, Jasne A, Zachariah CR, Rammohan K, Knopp MV, Schmalbrock P. Imaging cortical lesions in multiple sclerosis with ultra-high-field magnetic resonance imaging. Arch Neurol. Jul; 2010 67(7):812–8. http://-www.ncbi.nlm.nih.gov/pubmed/20625086. [PubMed: 20625086]

Polak, P., Zivadinov, R., Schweser, F. Proc Intl Soc Mag Reson Med. Vol. 23. Toronto, CA: 2015. 2015. Gradient Unwarping for Phase Imaging Reconstruction; p. 1279

Polman CH, Reingold SC, Banwell B, Clanet M, Cohen JA, Filippi M, Fujihara K, Havrdova E, Hutchinson M, Kappos L, Lublin FD, Montalban X, O'Connor P, Sandberg-Wollheim M, Thompson AJ, Waubant E, Weinshenker B, Wolinsky JS. Diagnostic criteria for multiple sclerosis: 2010 Revisions to the McDonald criteria. Ann Neurol. 2011; 69(2):292–302. [PubMed: 21387374]

Popescu BFG, Frischer JM, Webb SM, Tham M, Adiele RC, Robinson CA, Fitz-Gibbon PD, Weigand SD, Metz I, Nehzati S, George GN, Pickering IJ, Br?ck W, Hametner S, Lassmann H, Parisi JE, Yong G, Lucchinetti CF. Pathogenic implications of distinct patterns of iron and zinc in chronic MS lesions. Acta Neuropathologica. Jul; 2017 134(1):45–64. http://link.springer.com/10.1007/-s00401-017-1696-8. [PubMed: 28332093]

Postuma RB, Dagher A. Basal ganglia functional connectivity based on a meta-analysis of 126 positron emission tomography and functional magnetic resonance imaging publications. Cerebral Cortex. 2006; 16(10):1508–1521. [PubMed: 16373457]

Preziosa P, Pagani E, Mesaros S, Riccitelli GC, Dackovic J, Drulovic J, Filippi M, Rocca MA. Progression of regional atrophy in the left hemisphere contributes to clinical and cognitive deterioration in multiple sclerosis: A 5-year study. Human Brain Mapping. 2017 Jun.00 http://doi.wiley.com/10.1002/hbm.23755.

Quinn MP, Gati JS, Klassen ML, Lee DH, Kremenchutzky M, Menon RS. Increased deep gray matter iron is present in clinically isolated syndromes. Multiple Sclerosis and Related Disorders. 2014; 3(2):194–202. http://dx.doi.org/10.1016/-j.msard.2013.06.017. [PubMed: 25878007]

Ramasamy DP, Benedict RHB, Cox JL, Fritz D, Abdelrahman N, Hussein S, Minagar A, Dwyer MG, Zivadinov R. Extent of cerebellum, subcortical and cortical atrophy in patients with MS. A case-control study. Journal of the Neurological Sciences. 2009; 282(1–2):47–54. http://dx.doi.org/10.1016/j.jns.2008.12.034. [PubMed: 19201003]

Ramcharan EJ, Gnadt JW, Sherman SM. Higher-order thalamic relays burst more than first-order relays. Proceedings of the National Academy of Sciences of the United States of America. 2005; 102(34):12236–41. http://www.pubmedcentral.nih.gov/-articlerender.fcgi?artid=1189315&tool=pmcentrez&rendertype=abstract. [PubMed: 16099832]

Raz E, Branson B, Jensen JH, Bester M, Babb JS, Herbert J, Grossman RI, Inglese M. Relationship between iron accumulation and white matter injury in multiple sclerosis: a case???control study. J Neurol. 2014; 262(2):402–409. [PubMed: 25416468]

Reichenbach JR, Schweser F, Serres B, Deistung A. Quantitative Susceptibility Mapping: Concepts and Applications. Clin Neuroradiol. Oct; 2015 25(S2):225–230. http://link.springer.com/10.1007/s00062-015-0432-9.

Rissanen E, Tuisku J, Rokka J, Paavilainen T, Parkkola R, Rinne JO, Airas L. In Vivo Detection of Diffuse Inflammation in Secondary Progressive Multiple Sclerosis Using PET Imaging and the Radioligand C-11-PK11195. J Nucl Med. 2014; 55(6):939–944. http://www.ncbi.nlm.nih.gov/pubmed/24711650%5Cnhttp://-jnm.snmjournals.org/content/55/6/939.full.pdf%5Cn%3CGo to ISI%3E://-WOS:000336829900016. [PubMed: 24711650]

Rocca MA, Mesaros S, Pagani E, Sormani MP, Comi G, Filippi M. Thalamic Damage and Long-term Progression of Disability in Multiple Sclerosis. Radiology. 2010; 257(2):463–469. http://pubs.rsna.org/doi/10.1148/radiol.10100326. [PubMed: 20724544]

Rone MB, Cui QL, Fang J, Wang LC, Zhang J, Khan D, Bedard M, Almazan G, Ludwin SK, Jones R, Kennedy TE, Antel JP. Oligodendrogliopathy in Multiple Sclerosis: Low Glycolytic Metabolic Rate Promotes Oligodendrocyte Survival. Journal of Neuroscience. 2016; 36(17):4698–4707. http://www.jneurosci.org/cgi/-doi/10.1523/JNEUROSCI.4077-15.2016. [PubMed: 27122029]

Ropele, S., Enzinger, C., Fazekas, F. Iron Mapping in Multiple Sclerosis. Neuroimaging Clinics of North America. Jan. 2017 http://linkinghub.elsevier.com/retrieve/pii/-S1052514916301277

Rudko DA, Solovey I, Gati JS, Kremenchutzky M, Menon RS. Multiple Sclerosis: Improved Identification of Disease-relevant Changes in Gray and White Matter by Using Susceptibility-based MR Imaging. Radiology. Sep; 2014 272(3):851–864. http://pubs.rsna.org/doi/full/10.1148/radiol.14132475http://pubs.rsna.org/doi/abs/-10.1148/radiol.14132475. [PubMed: 24828000]

Santin MD, Didier M, Valabrègue R, Yahia Cherif L, García-Lorenzo D, Loureiro de Sousa P, Bardinet E, Lehéricy S. Reproducibility of R2* and quantitative susceptibility mapping (QSM) reconstruction methods in the basal ganglia of healthy subjects. NMR Biomed. Apr.2017 30(4):e3491. http://doi.wiley.com/10.1002/nbm.3491.

Schaltenbrand, G., Hassler, RG., Wahren, W. Architectonic organization of the thalamic nuclei by Rolf Hassler. 2nd. Thieme; Stuttgart, Germany: 1977. Atlas for stereotaxy of the human brain: with an accompanying guide.

Schenck JF. Health and physiological effects of human exposure to whole-body four-tesla magnetic fields during MRI. Ann N Y Acad Sci. Mar.1992 649:285–301. http://-www.ncbi.nlm.nih.gov/pubmed/1580500. [PubMed: 1580500]

Schmalbrock P, Prakash RS, Schirda B, Janssen A, Yang GK, Russell M, Knopp MV, Boster A, Nicholas JA, Racke M, Pitt D. Basal Ganglia Iron in Patients with Multiple Sclerosis Measured with 7T Quantitative Susceptibility Mapping Correlates with Inhibitory Control. Am J Neuroradiol. Mar; 2016 37(3):439–446. http://www.ajnr.org/cgi/doi/10.3174/ajnr.A4599. [PubMed: 26611996]

Schonberg DL, Goldstein EZ, Sahinkaya FR, Wei P, Popovich PG, McTigue DM. Ferritin stimulates oligodendrocyte genesis in the adult spinal cord and can be transferred from macrophages to NG2 cells in vivo. The Journal of neuroscience : the official journal of the Society for Neuroscience. 2012; 32(16):5374–84. http://www.ncbi.nlm.nih.gov/pubmed/22514302%5Cnhttp://-www.pubmedcentral.nih.gov/articlerender.fcgi?artid=PMC3521599. [PubMed: 22514302]

Schuitemaker A, Doef TFVD, Boellaard R, Jonker C, Kloet RW, Lammertsma AA, Scheltens P, Berckel BNMV. Microglial activation in healthy aging. Neurobiol Aging. 2012; 33(6):1067–1072. http://dx.doi.org/10.1016/-j.neurobiolaging.2010.09.016. [PubMed: 21051106]

Schweser F, Deistung A, Lehr BW, Reichenbach JR. Differentiation Between Diamagnetic and Paramagnetic Cerebral Lesions Based on Magnetic Susceptibility Mapping. Med Phys. 2010; 37(10):5165–5178. http://dx.doi.org/10.1118/1.3481505http://-www.ncbi.nlm.nih.gov/pubmed/21089750. [PubMed: 21089750]

Schweser F, Deistung A, Lehr BW, Reichenbach JR. Quantitative imaging of intrinsic magnetic tissue properties using MRI signal phase: An approach to in vivo brain iron metabolism? NeuroImage. Oct; 2011 54(4):2789–2807. http://-www.ncbi.nlm.nih.gov/pubmed/21040794http://dx.doi.org/10.1016/-j.neuroimage.2010.10.070. [PubMed: 21040794]

Schweser F, Deistung A, Reichenbach JR. Foundations of MRI phase imaging and processing for Quantitative Susceptibility Mapping (QSM). Z Med Phys. Mar; 2016 26(1):6–34. http://linkinghub.elsevier.com/retrieve/pii/S0939388915001427. [PubMed: 26702760]

Schweser, F., Poulsen, A., Shah, D., Bertolino, N., Preda, M., Kyyriäinen, J., Pitkänen, A., Zivadinov, R., Poulsen, DJ. Proc Intl Soc Mag Reson Med. Vol. 25. Honolulu, HI: 2017. 9.4 Tesla in vivo Quantitative Susceptibility Mapping (QSM) detects thalamic calcium influx associated with repeated mild traumatic brain injury (mTBI). 2017

Schweser F, Robinson SD, de Rochefort L, Li W, Bredies K. An illustrated comparison of processing methods for phase MRI and QSM: removal of background field contributions from sources outside the region of interest. NMR Biomed. Apr.2017 30(4):e3604. http://doi.wiley.com/10.1002/nbm.3604.

Schweser F, Sommer K, Deistung A, Reichenbach JR. Quantitative susceptibility mapping for investigating subtle susceptibility variations in the human brain. NeuroImage. Jun; 2012 62(3):2083–2100. http://linkinghub.elsevier.com/retrieve/pii/-S1053811912005551http://www.ncbi.nlm.nih.gov/pubmed/22659482. [PubMed: 22659482]

Sepulcre J, Murie-Fernandez M, Salinas-Alaman A, García-Layana A, Bejarano B, Villoslada P. Diagnostic accuracy of retinal abnormalities in predicting disease activity in MS. Neurology. 2007; 68(18):1488–1494. [PubMed: 17470751]

Sherman, SM., Guillery, RW. Functional Connections of Cortical Areas: A New View from the Thalamus. MIT Press; 2013. First and Higher Order Thalamic Relays; p. 119-141.Ch. 5.4.2.2

Sherman, SM., Guillery, RW. Functional Connections of Cortical Areas: A New View from the Thalamus. MIT Press; 2013. The Basic Organization of Cortex and Thalamus; p. 49-82.Ch. 3

Shipp S. The functional logic of cortico-pulvinar connections. Philosophical Transactions of the Royal Society B: Biological Sciences. 2003; 358(1438):1605–1624. http://rstb.royalsocietypublishing.org/cgi/doi/10.1098/rstb.2002.1213.

Smith SM, Zhang Y, Jenkinson M, Chen J, Matthews PM, Federico A, De Stefano N. Accurate, robust, and automated longitudinal and cross-sectional brain change analysis. NeuroImage. 2002; 17(1):479–89. http://www.ncbi.nlm.nih.gov/pubmed/-12482100. [PubMed: 12482100]

Sørensen J, Dalmau I, Zimmer J, Finsen B. Microglial reactions to retrograde degeneration of tracer-identified thalamic neurons after frontal sensorimotor cortex lesions in adult rats. Experimental Brain Research. Nov.1996 112(2) http://link.springer.com/-10.1007/BF00227639.

Spatz H. Über Stoffwechseleigentümlichkeiten in den Stammganglien. Zeitschrift für die gesamte Neurologie und Psychiatrie. Dec; 1922 78(1):641–648. http://link.springer.com/-10.1007/BF02867643.

Stephenson E, Nathoo N, Mahjoub Y, Dunn JF, Yong VW. Iron in multiple sclerosis: roles in neurodegeneration and repair. Nat Rev Neurol. Aug; 2014 10(8):459–68. http://www.ncbi.nlm.nih.gov/pubmed/25002107. [PubMed: 25002107]

Stepniewska, I. The Pulvinar Complex. In: Kaas, JH., Collins, CE., editors. The Primate Visual System. CRC Press; 2004. p. 53-80.Ch. 3

Straub, S., Laun, FB., Emmerich, J., Jobke, B., Hauswald, H., Katayama, S., Herfarth, K., Schlemmer, HP., Ladd, ME., Ziener, CH., Bonekamp, D., Röthke, MC. Potential of quantitative susceptibility mapping for detection of prostatic calcifications. J Magn Reson Imaging. Jul. 2016 (epub) http://doi.wiley.com/10.1002/-jmri.25385

Straub S, Schneider TM, Emmerich J, Freitag MT, Ziener CH, Schlemmer H-p, Ladd ME, Laun FB. Suitable reference tissues for quantitative susceptibility mapping of the brain. Magnetic Resonance in Medicine. Aug; 2016 00(9):3–6. http://doi.wiley.com/10.1002/mrm.26369.

Strijbis EMM, Inkster B, Vounou M, Naegelin Y, Kappos L, Radue EW, Matthews PM, Uitdehaag BMJ, Barkhof F, Polman CH, Montana G, Geurts JJG. Glutamate gene polymorphisms predict brain volumes in multiple sclerosis. Multiple sclerosis (Houndmills, Basingstoke, England). 2013; 19(3):281–8. http://www.ncbi.nlm.nih.gov/pubmed/22851457.

Stüber C, Morawski M, Schäfer A, Labadie C, Wähnert M, Leuze C, Streicher M, Barapatre N, Reimann K, Geyer S, Spemann D, Turner R. Myelin and iron concentration in the human brain: A quantitative study of MRI contrast. NeuroImage. Jun.2014 93:95–106. http://linkinghub.elsevier.com/retrieve/pii/-S1053811914001359. [PubMed: 24607447]

Stüber C, Pitt D, Wang Y. Iron in Multiple Sclerosis and Its Noninvasive Imaging with Quantitative Susceptibility Mapping. Int J Mol Sci. Jan.2016 17(1):100. http://-www.mdpi.com/1422-0067/17/1/100.

Sullivan EV, Rosenbloom M, Serventi KL, Pfefferbaum A. Effects of age and sex on volumes of the thalamus, pons, and cortex. Neurobiology of Aging. 2004; 25(2):185–192. [PubMed: 14749136]

Tourdias T, Saranathan M, Levesque IR, Su J, Rutt BK. Visualization of intra-thalamic nuclei with optimized white-matter-nulled MPRAGE at 7T. NeuroImage. 2014; 84:534–545. http://dx.doi.org/10.1016/j.neuroimage.2013.08.069. [PubMed: 24018302]

Trojano M, Lucchese G, Graziano G, Taylor BV, Simpson S, Lepore V, Maison FG, Duquette P, Izquierdo G, Grammond P, Amato MP, Bergamaschi R, Giuliani G, Boz C, Hupperts R. Geographical Variations in Sex Ratio Trends over Time in Multiple Sclerosis. PLoS ONE. 2012; 7(10):e48078. [PubMed: 23133550]

Unrath A, Klose U, Grodd W, Ludolph AC, Kassubek J. Directional colour encoding of the human thalamus by diffusion tensor imaging. Neuroscience Letters. 2008; 434(3):322–327. [PubMed: 18325671]

Vercellino M, Masera S, Lorenzatti M, Condello C, Merola A, Mattioda A, Tribolo A, Capello E, Mancardi GL, Mutani R, Giordana MT, Cavalla P. Demyelination, inflammation, and neurodegeneration in multiple sclerosis deep gray matter. J Neuropathol Exp Neurol. 2009; 68(5):489–502. [PubMed: 19525897]

Verkhratsky, A. Glial Physiology and Pathophysiology. John Wiley & Sons, Ltd; Chichester, UK: Feb. 2013 Oligodendrocytes; p. 245-319.http://doi.wiley.com/-10.1002/9781118402061.ch5

Wagenknecht N, Becker B, Scheld M, Beyer C, Clarner T, Hochstrasser T, Kipp M. Thalamus Degeneration and Inflammation in Two Distinct Multiple Sclerosis Animal Models. Journal of Molecular Neuroscience. 2016; 60(1):102–114. http://-dx.doi.org/10.1007/s12031-016-0790-z. [PubMed: 27491786]

Walsh AJ, Blevins G, Lebel RM, Seres P, Emery DJ, Wilman AH. Longitudinal MR imaging of iron in multiple sclerosis: an imaging marker of disease. Radiology. 2014; 270(1):186–96. http://www.ncbi.nlm.nih.gov/pubmed/23925273. [PubMed: 23925273]

Wang Y, Liu T. Quantitative susceptibility mapping (QSM): Decoding MRI data for a tissue magnetic biomarker. Magn Reson Med. 2015; 73(1):82–101. http://doi.wiley.com/-10.1002/mrm.25358. [PubMed: 25044035]

Wei H, Bonjean M, Petry HM, Sejnowski TJ, Bickford ME. Thalamic Burst Firing Propensity: A Comparison of the Dorsal Lateral Geniculate and Pulvinar Nuclei in the Tree Shrew. Journal of Neuroscience. 2011; 31(47):17287–17299. [PubMed: 22114295]

Wiegell MR, Tuch DS, Larsson HB, Wedeen VJ. Automatic segmentation of thalamic nuclei from diffusion tensor magnetic resonance imaging. NeuroImage. 2003; 19(2):391–401. http://linkinghub.elsevier.com/retrieve/pii/S1053811903000442. [PubMed: 12814588]

Winkler AM, Ridgway GR, Webster MA, Smith SM, Nichols TE. Permutation inference for the general linear model. NeuroImage. 2014; 92:381–397. http://-dx.doi.org/10.1016/j.neuroimage.2014.01.060. [PubMed: 24530839]

Wisnieff C, Ramanan S, Olesik J, Gauthier S, Wang Y, Pitt D. Quantitative susceptibility mapping (QSM) of white matter multiple sclerosis lesions: Interpreting positive susceptibility and the presence of iron. Magn Reson Med. Aug; 2015 74(2):564–570. http://www.ncbi.nlm.nih.gov/pubmed/25137340http://doi.wiley.com/10.1002/-mrm.25420. [PubMed: 25137340]

Wu B, Li W, Guidon A, Liu C. Whole brain susceptibility mapping using compressed sensing. Magn Reson Med. 2011; 24:1129–36. http://www.ncbi.nlm.nih.gov/-pubmed/21671269.

Wylezinska M, Cifelli AI, Jezzard P, Palace J, Alecci M, Matthews P. Thalamic neurodegeneration in relapsing: Remitting multiple sclerosis. Journal of Neurology Neurosurgery and Psychiatry. 2003; 74(8):1177.

Yao B, Hametner S, Gelderen PV, Merkle H, Chen C, Lassmann H, Duyn JH, Bagnato F. 7 Tesla Magnetic Resonance Imaging to Detect Cortical Pathology in Multiple Sclerosis. PloS one. 2014; 9(10)

Ystad M, Eichele T, Lundervold AJ, Lundervold A. Subcortical functional connectivity and verbal episodic memory in healthy elderly-A resting state fMRI study. NeuroImage. 2010; 52(1):379–388. http://dx.doi.org/10.1016/-j.neuroimage.2010.03.062. [PubMed: 20350608]

Ystad M, Hodneland E, Adolfsdottir S, Haász J, Lundervold AJ, Eichele T, Lundervold A. Cortico-striatal connectivity and cognition in normal aging: A combined DTI and resting state fMRI study. NeuroImage. 2011; 55(1):24–31. http://-dx.doi.org/10.1016/j.neuroimage.2010.11.016. [PubMed: 21073962]

Zhang X, Haaf M, Todorich B, Grosstephan E, Schieremberg H, Surguladze N, Connor JR. Cytokine toxicity to oligodendrocyte precursors is mediated by iron. Glia. 2005; 52(3):199–208. [PubMed: 15968631]

Zhang X, Surguladze N, Slagle-Webb B, Cozzi A, Connor JR. Cellular iron status influences the functional relationship between microglia and oligodendrocytes. Glia. Dec; 2006 54(8):795–804. http://doi.wiley.com/10.1002/glia.20416. [PubMed: 16958088]

Zhang Y, Gauthier SA, Gupta A, Chen W, Comunale J, Chiang GCY, Zhou D, Askin G, Zhu W, Pitt D, Wang Y. Quantitative Susceptibility Mapping and R2* Measured Changes during White Matter Lesion Development in Multiple Sclerosis: Myelin Breakdown, Myelin Debris Degradation and Removal, and Iron Accumulation. Am J Neuroradiol. Sep; 2016 37(9):1629–1635. http://www.ajnr.org/cgi/doi/-10.3174/ajnr.A4825. [PubMed: 27256856]

Zheng W, Nichol H, Liu S, Cheng YCN, Haacke EM. Measuring iron in the brain using quantitative susceptibility mapping and X-ray fluorescence imaging. NeuroImage. Apr.2013 78:68–74. http://www.ncbi.nlm.nih.gov/pubmed/23591072http://-www.pubmedcentral.nih.gov/-articlerender.fcgi?artid=3843006&tool=pmcentrez&rendertype=abstract. [PubMed: 23591072]

Zhou Q, Godwin DW, O'Malley DM, Adams PR. Visualization of calcium influx through channels that shape the burst and tonic firing modes of thalamic relay cells. Journal of neurophysiology. 1997; 77(5):2816–2825. http://www.ncbi.nlm.nih.gov/-pubmed/9163395%5Cnhttp://jn.physiology.org/content/77/5/2816.short. [PubMed: 9163395]

Zivadinov R, Bergsland NP, Cappellani R, Hagemeier J, Melia R, Carl E, Dwyer MG, Lincoff N, Weinstock-Guttman B, Ramanathan M. Retinal nerve fiber layer thickness and thalamus pathology in multiple sclerosis patients. European Journal of Neurology. Aug; 2014 21(8):1137–e61. http://www.ncbi.nlm.nih.gov/pubmed/-24779967http://doi.wiley.com/10.1111/ene.12449. [PubMed: 24779967]

Zivadinov R, Havrdová E, Bergsland NP, Tyblova M, Hagemeier J, Seidl Z, Dwyer MG, Vaneckova M, Krasensky J, Carl E, Kalincik T, Horáková D. Thalamic atrophy is associated with development of clinically definite multiple sclerosis. Radiology. 2013; 268(3):831–41. http://www.ncbi.nlm.nih.gov/pubmed/23613615. [PubMed: 23613615]

Zivadinov R, Heininen-Brown M, Schirda CV, Poloni GU, Bergsland NP, Magnano CR, Durfee J, Kennedy C, Carl E, Hagemeier J, Benedict RHB, Weinstock-Guttman B, Dwyer MG. Abnormal subcortical deep-gray matter susceptibility-weighted imaging filtered phase measurements in patients with multiple sclerosis: a case-control study. NeuroImage. Jan; 2012 59(1):331–9. http://-www.ncbi.nlm.nih.gov/pubmed/21820063. [PubMed: 21820063]

Zivadinov R, Schirda C, Dwyer MG, Haacke EM, Weinstock-Guttman B, Menegatti E, Heininen-Brown M, Magnano CR, Malagoni aM, Wack DS, Hojnacki D, Kennedy C, Carl E, Bergsland NP, Hussein S, Poloni GU, Bartolomei I, Salvi F, Zamboni P. Chronic cerebrospinal venous insufficiency and iron deposition on susceptibility-weighted imaging in patients with multiple sclerosis: a pilot case-control study. Int Angiol. Apr; 2010 29(2):158–75. http://www.ncbi.nlm.nih.gov/-pubmed/20351672. [PubMed: 20351672]

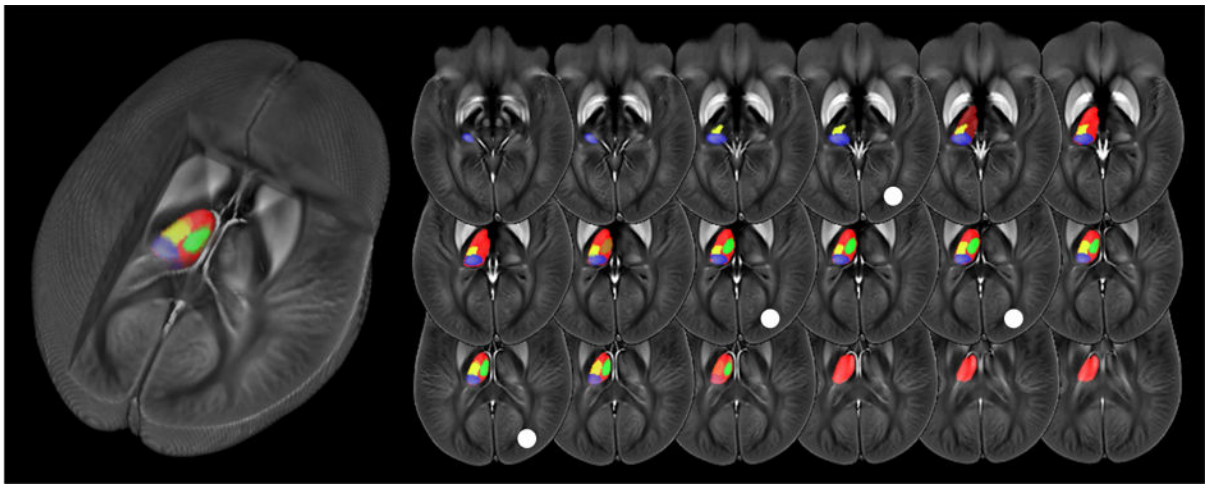

Figure 1.

Brain template and custom thalamus atlas. Pulvinar (PUL) indicated in blue, lateral nuclear region (LNR) in yellow, and medial nuclear region (MNR) in green. The global thalamus (GT) is indicated in red (other areas overlaid). The white circle indicates the location of the slices used in the enlarged views in Fig. 2. The cutout view on the left visualizes the three-dimensional spatial location in the brain.

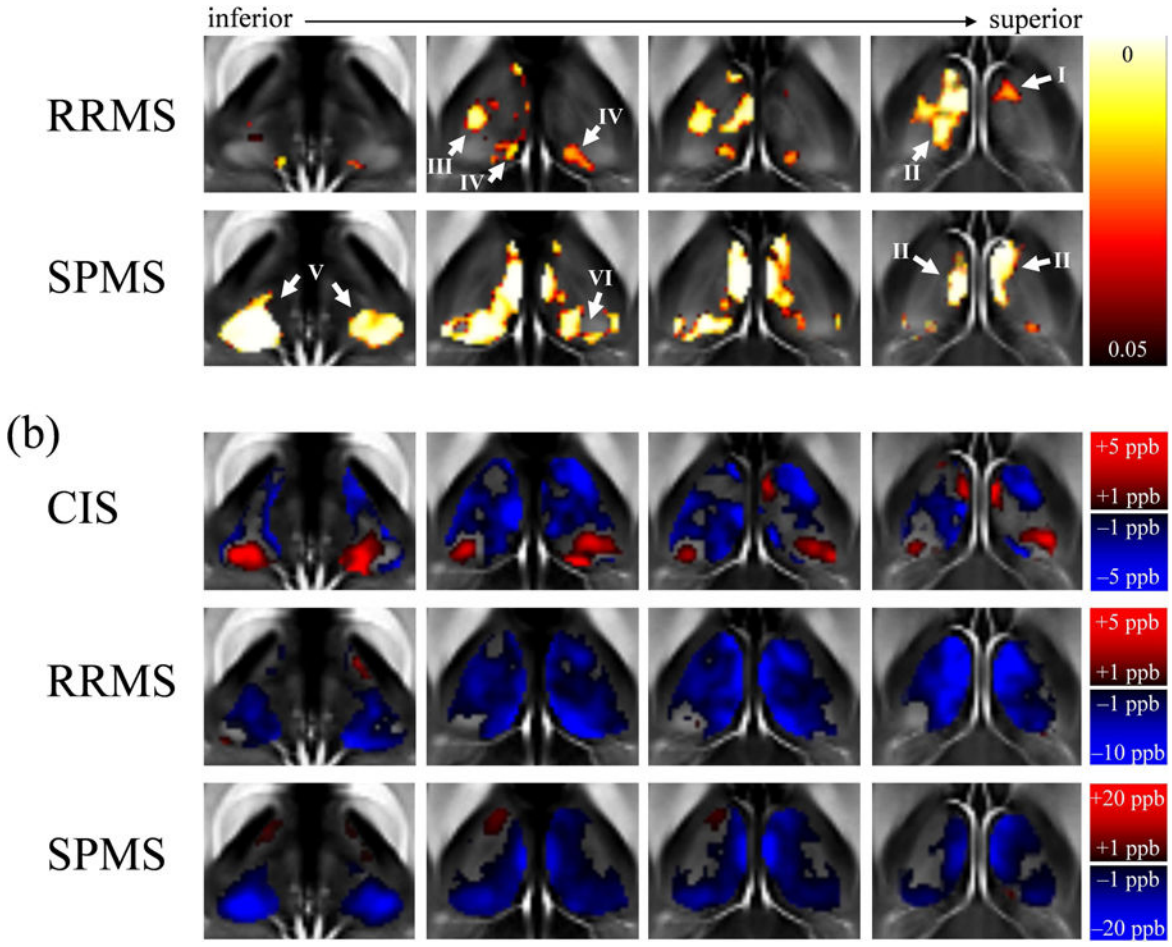

Figure 2.

Results of the voxel-based analysis. (a) Regions in which differences between patients and controls reached statistical significance. Shown are voxels with a p-value below 0.05 (color-coding) after TFCE in selected slices (white circles in Fig. 1). The corresponding overview of the results in the whole thalamus is shown in Fig. S.3 in the Supplementary Material. (b) Voxel-based group-average differences of magnetic susceptibility between the patient and their corresponding NC groups (top to bottom) in selected slices, illustrating the magnitude and direction of the group differences in every voxel. Note the differences in contrast between the groups (color bars). The corresponding overview of the results in the whole thalamus is shown in Fig. S.4 along with the Z-scores

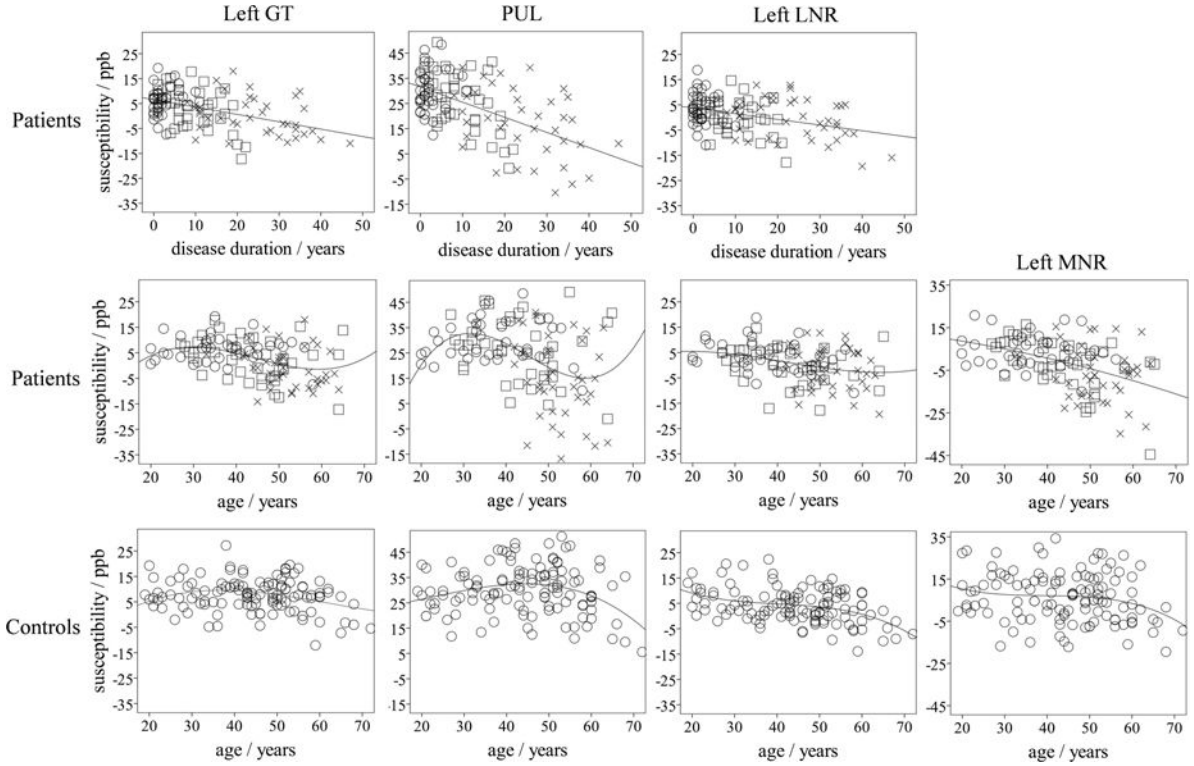

Figure 3.

Top and middle row: Scatter plots illustrating univariate associations of susceptibility for regions that were significant in the multivariate analysis (top row and middle row for patients) and, for illustrative purposes, associations with age for the same regions (middle row). The shapes of the markers indicate the clinical phenotypes: circle – CIS; square – RRMS; cross - SPMS. In the top row, linear regression curves are used, whereas in the middle row cubic curves were used, except for the MNR, where we used a quadratic fit. Bottom row: Scatter plots of the susceptibilities in corresponding regions of NCs over age. The regression line for the left GT was determined by fitting $a + b \cdot (0.3\ \text{mg/100g} \cdot age - 5.82 \cdot 10^{-3}\ \text{mg/100g} \cdot age^2 + 3.15 \cdot 10^{-5}\ \text{mg/100g} \cdot age^3)$ to the susceptibility values (Levenberg-Marquardt), which relies on the known iron aging-trajectory in the GT (see Figure S.6 in the Supplementary Material). The fitted coefficients were $a = (-15.3 \pm 6.9)$ ppb and $b = (5.22 \pm 1.58)$ ppb·100g/mg. For the other NC plots, we used a cubic regression (PUL: R^2=0.13, ANOVA p=0.0011, $22.0\text{ppb} - 7.18 \cdot 10^{-3}\ \text{ppb/a} \cdot \text{age} + 1.62 \cdot 10^{-2}\ \text{ppb/a}^2 \cdot \text{age}^2 - 2.41 \cdot 10^{-4}\ \text{ppb/a}^3 \cdot \text{age}^3$; MNR: R^2=0.05, p=0.11; LNR: R^2=0.22, p<0.001, $20.3\text{ppb} - 8.36 \cdot 10^{-1}\ \text{ppb/a} \cdot \text{age} + 1.77 \cdot 10^{-2}\ \text{ppb/a}^2 \cdot \text{age}^2 - 1.48 \cdot 10^{-4}\ \text{ppb/a}^3 \cdot \text{age}^3$). For improved visualization, all ordinates, except that of the MNR, cover a susceptibility interval of 65ppb (all data points are visible).

Table 1

Demographics and clinical details of the study groups in this work.

	Patients			Normal controls (NC)				
	CIS	**RRMS**	**SPMS**	**CIS-NC**	**RRMS-NC**	**SPMS-NC**	**All patients**	**All NCs**
N	40	40	40	40	40	40	120	120
Age (years)	36.9±9.8 [20–58]	43.6±10. [27–65]	52.0±7.0 [33–64]	37.0±11.6 [20–59]	44.0±10.0 [19–60]	52.6±11.9 [23–76]	44.1±10.9 [20–65]	44.5±12.8 [19–76]
Sex ratio (F/M)	29:11	27:13	29:11	28:12	30:10	29:11	85:35	87:33
EDSS	1.5, 0.5–2.5	2.0, 1–3	6.5, 4–9	–	–	–	2.5, 0–7	–
dd (years)	2.2±2.6	9.8±6.0	24.0±10.2	–	–	–	11.9±11.4	–

Values stated as *n, m-p* represent median, IQR; *n*±*m* indicates mean and standard deviation; [*m-p*] indicates The range. The abbreviation dd stands for disease duration and *N* is the number of subject.

Table 2

Average magnetic susceptibility (parts-per-billion; ppb) in thalamic subnuclei.

	CIS-NC	CIS	RRMS-NC	RRMS	SPMS-NC	SPMS
GT						
Avg (CI)			9.2 ± 6.0 (1.85)	3.3 ± 3.3 (1.85)	7.08±5.7 (1.76)	0.079±6.1 (1.90)
Left (CI)	7.4 ± 7.2 (2.23)	6.1 ± 5.2 (1.6)				
Right (CI)	10.0 ± 5.3 (1.63)	9.0 ± 4.7 (4.7)				
Difference *(d)*	−1.3 (−0.21) / −1 (−0.20)		−5.9 (−0.86)		−7.0 (−1.18)	
p	0.34 / 0.37		**<0.001****		**<0.001****	
PUL						
Avg (CI)	29.2 ± 9.2 (2.85)	30.4 ± 8.2 (2.54)	30.9 ± 9.3 (2.90)	25.6±11.4 (3.55)	29.9±10.4 (3.21)	16.6±13.6 (4.21)
Difference (*d*)	+1.2 (0.14)		−5.3 (−0.50)		−13.3 (−1.10)	
p	0.56		0.028*		**<0.001****	
MNR						
Avg (CI)					3.9 ± 11.2 (3.48)	−7.8±12.1 (3.74)
Left (CI)	6.7 ± 13.2 (4.09)	4.3 ± 7.7 (2.39)	7.3 ± 10.8 (3.91)	−2.4±12.4 (3.80)		
Right (CI)	6.1 ± 9.5 (2.95)	6.9 ± 8.5 (2.63)	4.7 ± 12.6 (3.91)	−3.1±14.9 (4.60)		
Difference (*d*)	−2.4 (−0.23) / 0.8 (0.08)		−9.7 (−0.84) / −7.8 (−0.57)		−11.·7 (−1.00)	
p	0.30 / 0.74		**<0.001***/0.019*		**<0.001****	
LNR						
Avg (CI)					2.6 ± 5.0 (1.56)	0.19 ± 5.8 (1.81)
Left (CI)	5.2 ± 7.1 (2.20)	3.6 ± 6.0 (1.85)	4.9 ± 6.5 (2.01)	−0.2 ± 7.1 (2.21)		
Right (CI)	7.9 ± 5.4 (1.68)	5.9 ± 5.4 (1.68)	5.6 ± 7.2 (2.22)	2.5 ± 6.9 (2.15)		
Difference (*d*)	−1.6 (−0.24) / −2.0 (−0.36)		−5.1 (−0.75) / −3.1 (−0.44)		−2.41 (−0.44)	
p	0.28 / 0.11		**0.001*** / 0.058		0.051	

Values are reported as mean ± standard deviation. CI denotes the 95% confidence interval, *d* is Cohen's effect size. For each region, values are reported either as bi-hemispheric average (Avg) or for each hemisphere individually, depending on the statistical significance of differences between hemispheres. If sample distributions were different in either the patient or the control groups, hemispheres were analyzed separately for both groups. All sample distributions were normal. For the comparisons of hemispheres, differences are reported as left / right. The *p*-values were determined by univariate ANCOVA

adjusted for sex (we found no significant interactions with sex except for a trend in the right MNR with p=0.042). Bonferroni corrected thresholds for statistical significance were 0.05/7=0.0071 for CIS, 0.05/6=0.0083 for RRMS, and 0.05/4=0.0125 for SPMS. Trends are indicated by *, statistical significance after Bonferroni correction is indicated by ** and boldface.

Table 3

Average volumes (in milliliters; ml) in thalamic subnuclei.

	CIS-NC	CIS	RRMS-NC	RRMS	SPMS-NC	SPMS
GT						
Sum (CI)			16.81 ± 0.13 (0.416)	14.90 ± 1.72 (0.531)	16.07 ± 1.31 (0.407)	14.00 ± 1.85 (0.572)
Left (CI)	8.22 ± 0.64 (0.200)	8.05 ± 0.71 (0.221)				
Right (CI)	8.45 ± 0.53 (0.165)	8.17 ± 0.68 (0.211)				
Difference *(d)*	−0.17 (−0.25) / −0.28 (−0.47)		−1.91 (−1.2)		−2.07 (−1.1)	
p	0.28 / 0.043*		**<0.001***		**<0.001***	
PUL						
Left (CI)	2.14 ± 0.32 (0.0982)	2.05 ± 0.30 (0.0918)	2.22 ± 0.30 (0.0925)	1.84 ± 0.35 (0.109)	2.05 ± 0.27 (0.0833)	1.71 ± 0.38 (0.117)
Right (CI)	2.35 ± 0.29 (0.0904)	2.20 ± 0.33 (0.101)	2.39 ± 0.29 (0.0885)	2.01 ± 0.35 (0.109)	2.25 ± 0.29 (0.0899)	1.88 ± 0.41 (0.128)
Difference (*d*)	−0.09 (−0.30) / −0.15 (−0.49)		−0.38 (−1.1) / −0.38 (−1.2)		−0.34 (−1.0) / −0.37 (−1.0)	
p	0.19 / 0.034*		**<0.001*** / **<0.001***		**<0.001*** / **<0.001***	
MNR						
Left (CI)	0.79 ± 0.12 (0.0380)	0.77 ± 0.13 (0.0405)	0.78 ± 0.13 (0.0395)	0.69 ± 0.11 (0.0345)	0.76 ± 0.15 (0.0474)	0.64 ± 0.14 (0.0427)
Right (CI)	0.87 ± 0.10 (0.0326)	0.85 ± 0.12 (0.0385)	0.85 ± 0.16 (0.0500)	0.75 ± 0.15 (0.0461)	0.81 ± 0.14 (0.0424)	0.67 ± 0.12 (0.0365)
Difference (*d*)	−0.02 (−0.21) / −0.02 (−0.15)		−0.09 (−0.75) / −0.10 (−0.60)		−0.12 (−0.82) / −0.14 (−0.82)	
p	0.36 / 0.50		**0.0013*** / 0.012*		**<0.001*** / **<0.001***	
LNR						
Sum (CI)	2.063 ± 0.187 (0.0580)	2.035 ± 0.22 (0.0692)	2.10 ± 0.23 (0.0717)	1.83 ± 0.26 (0.0817)	2.00 ± 0.21 (0.0660)	1.69 ± 0.29 (0.0901)
Difference (*d*)	−0.024 (−0.086)		−01.26 (−1.0)		−0.36 (−1.1)	
p	0.56		**<0.001***		**<0.001***	

Values are reported as mean ± standard deviation. CI denotes the 95% confidence interval, *d* is Cohen's effect size. For each region, values are reported either as bi-hemispheric sum or for each hemisphere individually, depending on the statistical significance of differences between hemispheres. If sample distributions were different in either the patient or the control groups, hemispheres were analyzed separately for both groups. All sample distributions were normal, except the left and right PUL in SPMS (compared using Wilcoxon test). For the comparison of hemispheres, differences are reported as left / right. The *p*-values were determined by univariate ANCOVA adjusted for sex (we found no significant interactions with sex except for a trend in the right MNR with $p=0.027$). Bonferroni corrected thresholds for statistical significance were 0.05/7=0.0071 for CIS, 0.05/6=0.0083 for RRMS and SPMS. * indicates trends, statistical significance after Bonferroni correction is indicated by ** and boldface.

Table 4

Spearman rank correlation coefficients for volumes and susceptibility.

	CIS-NC	CIS	RRMS-NC	RRMS	SPMS-NC	SPMS
GT	0.249 (0.12)	0.328 (0.039*)	0.237 (0.14)	0.333 (0.036*)	0.390 (0.013*)	0.347 (0.028*)
PUL	0.379 (0.016*)	**0.419 (0.007**)**	0.315 (0.048*)	**0.539 (<0.001**)**	**0.414 (0.008**)**	**0.399 (0.011**)**
MNR	0.237 (0.14)	0.332 (0.037*)	**0.508 (0.001**)**	0.384 (0.014*)	**0.525 (0.001**)**	0.390 (0.013*)
LNR	0.163 (0.315)	0.110 (0.50)	0.222 (0.17)	0.111 (0.49)	0.292 (0.068)	0.234 (0.15)

P-values are shown in parentheses. Bonferroni corrected threshold for statistical significance was 0.05/4=0.0125 for each group. * indicates trends, statistical significance after Bonferroni correction is indicated by ** and boldface.